Student thesis series INES nr 563

Mapping future floods in coastal Bangladesh

Impacts of projected changes in sea level and precipitation

Agnes Pierre

2022
Department of
Physical Geography and Ecosystem Science
Lund University
Sölvegatan 12
S-223 62 Lund
Sweden

Agnes Pierre (2022).
Mapping of future floods in coastal Bangladesh - Impacts of projected changes in sea level and precipitation
Bachelor degree thesis, 15 credits in Physical Geography and Ecosystem Science
Department of Physical Geography and Ecosystem Science, Lund University

Level: Bachelor of Science (BSc)

Course duration: *January* 2022 until *June* 2022

Disclaimer

Mapping future floods in coastal Bangladesh
- Impacts of projected changes in sea level and precipitation

---

Agnes Pierre

Bachelor thesis, 15 credits, in Physical Geography and Ecosystem Science

Supervisor:
Marko Scholze
Department of Physical Geography and Ecosystem Science, Lund University

Exam committee:
Harry Lankreijer, Lund University
Hans Chen, Lund University

Acknowledgements

Thanks to my supervisor, Marko Scholze, for guidance and great inputs throughout the process. A special thank you to Petter Pilesjö and Andreas Persson at the Lund University GIS Centre, for introducing and providing access to the TFM-DYN model and for being available for discussions when needed.

Abstract

The exposure to flooding in coastal Bangladesh is expected to increase throughout the century as a result of climate change-induced sea level rise and intensified monsoon precipitation. The current consequences of flooding include damage to infrastructure, economy, and health through inundation and saline intrusion, and are likely to affect a larger population in the future. Adequate flood modelling using updated climate projections on a sub-national scale is thereby crucial to understand the impacts of climate change-induced flooding compared to today.

The change in flood extent and depth by 2080 relative to 2010 has been modelled and mapped using CMIP6 climate projections of sea level rise and precipitation for the intermediate radiative forcing scenario SSP2-4.5, high SSP3-7.0, and very high SSP5-8.5, using both mean end extreme projections for each scenario. Precipitation-induced flooding was simulated using the triangular form-based multiple flow algorithm TFM-DYN, and coastal inundation at high tide was generated through a passive flood modelling approach that incorporates sea level rise, land subsidence, and tidal influence.

The results are presented for a rural area in central coastal Bangladesh and suggest that both flood extent and depth are likely to increase across all SSP scenarios. Whilst smaller changes were observed for mean scenarios, the extreme scenarios resulted in the highest increase in flood extent and depth, where depth increased with higher magnitudes compared to extent. The findings highlight how floods in central coastal Bangladesh could become affected in a future climate, and can be considered for identification of flood-exposed areas.

Keywords: flood modelling, TFM-DYN, relative sea level rise, extreme precipitation, tidal inundation

Table of Contents

Abbreviations

BBS	Bangladesh Bureau of Statistics.
CCKP	Climate Change Knowledge Portal.
CMIP	Coupled Model Intercomparison Project.
DEM	Digital elevation model.
FAO	Food and Agriculture Organization of the United Nations.
GCM	General circulation model.
GBM	Ganges-Brahmaputra-Meghna.
GIS	Geographical information systems.
MDP	Mean daily precipitation
MSL	Mean sea level.
MX1day	Average largest 1-day precipitation.
IDF	Intensity-duration-frequency.
IPCC	Intergovernmental Panel on Climate Change.
RCP	Representative Concentration Pathway.
SRTM	Shuttle Radar Topography Mission.
SLR	Sea level rise.
SSP	Shared socioeconomic pathways.
TFM	Triangular form-based multiple flow algorithm.
WRI	World Resources Institute.

1 Introduction

Global sea levels are rising with high confidence and will continue to rise at an accelerating rate as global temperatures are increasing (IPCC, 2021). The increase in temperature leads to thermal expansion of the oceans and an increase in meltwater contribution from glaciers and ice sheets. Whilst climate models are improving at accurately modelling historical climate and projecting future climate with high confidence, even high sea level rise (SLR) scenarios of 2 m by 2100 and 5 m by 2150 cannot be ruled out due to large uncertainties in modelling of glaciers and ice-sheet dynamics (IPCC, 2021). SLR is regionally exacerbated by land subsidence, which has the potential to double projected SLR in coastal Bangladesh by the end of the century (Becker et al., 2020). It varies regionally between 1-18 mm/year across Bangladesh due to tectonic activity, sediment compaction and accumulation, groundwater extraction, and agricultural practices (Becker et al., 2020). The high uncertainties with future projections of SLR are hazardous for flood prone, low-lying countries such as Bangladesh, considering the combined effect of SLR and land subsidence and the already heavy monsoon precipitation is projected to increase in intensity and frequency (IPCC, 2021).

Bangladesh is located in the low-lying floodplain of the world's largest delta, Ganges-Brahmaputra-Meghna (GBM), which transports runoff water from the Himalayas into the Bay of Bengal. It hosts one of the largest population densities in the world in an area where 10% is found less than 1 m above mean sea level (MSL), thereby being vulnerable to coastal flooding (Becker et al., 2020). The climate is highly influenced by monsoon patterns, and 80% of the annual precipitation is received in torrential rains during the monsoon, coinciding with the highest annual temperatures (Climate Change Knowledge Portal [CCKP], 2021). The highest amounts of rain are generally received in July, which additionally is the time when tropical cyclones often make landfall and high river discharge occurs in the rivers, resulting in high risks of flooding (CCKP, 2021). The fertile delta favours the large agricultural sector that contributes 17.5% to the total GDP, provides about 50% of the population with employment, and occupies about 70% of the total area in Bangladesh (Food and Agriculture Organization of the United Nations [FAO], 2022). This economic asset is, however, threatened by waterlogging and saline intrusion from severe weather and climate events like extreme precipitation, SLR, and cyclones that result in yield loss and challenges food security and export (Bangladesh Bureau of Statistics [BBS], 2021).

One third of the population live in coastal Bangladesh and is particularly exposed to the risks of SLR (Asian Development Bank, 2021). The direct effect of SLR is coastline retreat, which in turn results in loss of habitable areas and increased extent of saline intrusion and contamination of groundwater (Ministry of Foreign Affairs of the Netherlands, 2021). This impacts the vast population in terms of economic damage and health risks (Bricheno et al., 2021; Dasgupta et al., 2018). Coastline retreat in turn increases the area prone to coastal flooding from daily tidal inundation, storm surge inundation, and tropical cyclones, and the consequences of SLR can thereby affect areas far inland.

Not only is global warming likely to increase the frequency and severity of coastal flooding with relative SLR, but monsoon rainfall is also projected to increase in intensity and frequency, resulting in exposure to flooding induced by extreme precipitation events (IPCC, 2021). Extreme precipitation events already occur in Bangladesh and have inundated vast areas of the country and affected millions of people (Dastagir, 2015). These two consequences of the ongoing global change pose a large flood threat to coastal Bangladesh, and without relevant adaptation, large areas of coastal Bangladesh are at risk of becoming inundated.

Most of the existing flood modelling studies in Bangladesh have been conducted on a national scale according to older climate projections, with the exception of regional studies focusing on riverine flooding in northern Bangladesh, coastal flooding in the Sundarbans, and

precipitation-induced flooding in Dhaka (Hasan et al., 2020; Murshed et al., 2011; Roy et al., 2021). This leaves a research gap for regional flood modelling in central coastal Bangladesh to investigate how climate change could affect tidal and precipitation- induced flooding using updated future climate projections.

1.1 Study aim and objectives

The aim of the thesis is to investigate the change in flood extent and depth from precipitation-induced flooding and coastal tidal flooding in coastal Bangladesh by 2080. The analysis will assess the change in July, which currently experiences a high occurrence of heavy rainfalls and flooding. This will be achieved using future IPCC projections of rainfall and relative SLR for mean and extreme events given the shared socioeconomic pathways (SSP) SSP2-4.5, SSP3-7.0, and SSP5-8.5. First, future areas flooded at high tide will be estimated through a passive flood modelling approach that incorporates SLR, land subsidence, and tide. Second, precipitation events will be simulated on the future landscapes using the multiple flow algorithm TFM-DYN to assess precipitation-induced flooding (Nilsson et al., 2021; Pilesjö & Hasan, 2014).

1.2 Hypothesis

i. The area of land inundated by relative SLR at high tide will increase across all scenarios and become greater with higher SSP scenarios. Change in flood extent is expected to be observed considering the flat landscape in coastal Bangladesh where small changes in elevation occur.

ii. Precipitation-induced flood depth and extent will increase with higher SSP. Higher amounts of rain are expected to result in higher flood extent and area inundated with higher depths if the other landscape features, such as land cover, infiltration, and surface roughness, remain unchanged.

iii. Precipitation-induced flood depths will change more than the spatial extent of the flood (Dasgupta et al., 2010).

iv. Extreme scenarios will lead to greater change compared to mean scenarios (CCKP, 2021).

1.3 Delineations

Some assumptions are made to limit the scope of the study. First, this thesis assumes no change in land use to occur by 2080 and thereby that agriculture will continue to occupy most of the rural landscape and be the main source of income in rural coastal regions. Second, the influence of high river discharge in the Meghna River, which is situated next to the study site, is not included in the study. It has, however, the potential to raise water levels up to 4 m in the delta which can expose the low coastline to flooding (Bricheno & Wolf, 2018). Third, the impact of coastal erosion on coastline retreat is additionally excluded from the scope.

2 Background

2.1 Historical precipitation-induced flooding

Bangladesh frequently experiences extreme precipitation events that result in flooding during the monsoon. About 21% of Bangladesh is flooded annually during the monsoon and 60% is flooded every 5 years during severe floods (Dastagir, 2015). The impacts of flooding resulting

from long extreme precipitation events involve excessive damage to housing, infrastructure, agriculture, health, and economy for millions of people (Dastagir, 2015).

Some historical precipitation-induced floods have been more extensive and caused more damage than others. In 2004, a long heavy precipitation event which inundated 39% of the country and left 30 million people homeless in Bangladesh culminated in 341 mm/day in Dhaka, which corresponds to a rain that statistically occurs once every 100 years (Dasgupta et al., 2015; Dastagir, 2015). A similar event in 2007 inundated 42% of Bangladesh and affected 14 million people in total, and 408 mm/day of rain was reported in Chittagong that suffered from deadly landslides as a result (Dastagir, 2015; Murshed et al., 2011). In 2009, a new record was set in Dhaka when 333 mm was reported within 12 hours, of which 290 mm occurred within 6 hours. Two of the most extensive floods occurred in 1988 and 1998, where 63% and 69% of Bangladesh was inundated respectively (Dastagir, 2015). In 1988, the floods damaged 2.12 million ha of crops, and water depths up to 4.5 m were measured in Dhaka where 85% of the city was flooded.

2.2 Consequences of sea level rise

One of the major threats with SLR is the resulting saline intrusion which has large consequences for the population in coastal Bangladesh. Saline intrusion is currently increasing annually in the GBM delta, and this trend is projected to continue to increase with future SLR (Dasgupta et al., 2018). Saline intrusion is a major issue for the agricultural sector that Bangladesh relies on since it restricts crop production and reduces soil fertility, resulting in reduced yields and economic consequences for local farmers (BBS, 2021; Dasgupta et al., 2018). This issue is exacerbated by the common use of river water for irrigation of cultivated areas, which also is contaminated by saline intrusion and in some areas have salt concentrations that even exceed the critical threshold for salt-resistant crop variants (Bricheno et al., 2021). The ongoing SLR is additionally leading to a reduction of suitable agricultural land in Bangladesh since coastline retreat allows for increased saline intrusion, and about 40% of coastal and offshore areas are already experiencing soil salinity (Ministry of Foreign Affairs of the Netherlands, 2018).

Whilst the government is researching on and suggesting adaptation strategies to farmers, these are not always implemented locally due to knowledge gaps and communication barriers (Dasgupta et al., 2018). One adaptation strategy amongst farmers is the change into saltwater aquaculture, such as shrimp farming (Bricheno et al., 2021). This practice benefits from increasing saline intrusion and provides farmers with stable income yet it contributes to exacerbate saline intrusion.

As relative SLR increases, saline ocean water will continue to expand inland and contaminate new areas and groundwater reserves. About 2.5 million ha of coastal Bangladesh already have groundwater salinity levels above the critical threshold for drinking water, and a continued depletion of groundwater reserves and consumption of saline drinking water has dire health consequences for the population (Bricheno et al., 2021).

The shift in coastlines resulting from regional SLR could lead to extensive flooding when combined with compound effects such as tropical cyclones, tidal contribution, and storm surges. Historical large-scale inundation has left millions of people homeless and threatened their livelihoods, and this problem is projected to increase with future coastline retreat.

2.3 Previous flood modelling studies

Many of the existing studies on modelling flood extent and depth following projections of future SLR and changed precipitation patterns have been conducted using older IPCC scenarios of global warming or set values of SLR.

A national-scale study by Hasan et al. (2020) has shown that a 1 m SLR by 2100 could inundate 4.9% of coastal Bangladesh. Brown et al. (2018) used IPCC's previous socio-

economic scenarios Special Report on Emissions Scenarios (SRES) for projections of various climate variables and SLR and reported that coastal Bangladesh would experience a doubling in flood extent for global warming of 3°C compared to 1.5°C.

The research conducted on change in flood depth following projected changes in climate, including precipitation patterns, agree on the conclusion that an increase of flood depth is more hazardous than an increase in inundation extent. Brown et al. (2018) reports a 50% increase in flood depth for unprotected areas in coastal Bangladesh with global warming of 3°C compared to 1.5°C. Dasgupta et al. (2010) states that flood extent will not change significantly by 2050 under the SRES A2 scenario, which resembles SSP3, however flood depths above 0.9 m could increase to occur in 40% of Bangladesh. This is supported by Roy et al. (2021) who state that flood depth will increase more than inundation extent and furthermore have more catastrophic effects.

3 Data and Methodology

3.1 Study site

The study was conducted in a catchment in central coastal Bangladesh (Figure 1). It covers 936 ha of which 57% is located below 7 m above MSL and 7% below 5 m. The catchment is located in the Lakshmipur district, which in turn is found in the division Chittagong, and it borders the Meghna River to the west. The district was chosen based on its vulnerability to ocean related hazards such as SLR and tidal flooding. Most of the coastal areas in central Bangladesh are furthermore unprotected to rising sea levels (Brown et al., 2018). The study site was chosen based on having the most low-lying landscape along the coastline, and furthermore for being representative of many rural coastal areas in Bangladesh. 85% of the study site is occupied by agriculture and is ranked as highly vulnerable to coastal flooding and SLR hazards (Asian Development Bank, 2021).

Lakshmipur is mainly agricultural and largely occupied with rice plantations, with smaller areas occupied by aquaculture (BBS, 2021). The district is representative for rural coastal areas in central Bangladesh with its highly agricultural landscape and poor population with low literacy rates below 50%, that is highly exposed and vulnerable to SLR, cyclones, tidal surge, and increasing soil salinity (Asian Development Bank, 2021; BBS, 2021; World Bank, 2011).

The division Chittagong receives on average 1500 mm of rainfall annually, and the highest monthly rainfall usually occur in July which receives on average 650 mm (CCKP, 2021). The highest amount of rainfall occurs during the monsoon from June-September. This coincides with the warmest months and mean daily temperatures above 27 °C are common from April - October (CCKP, 2021).

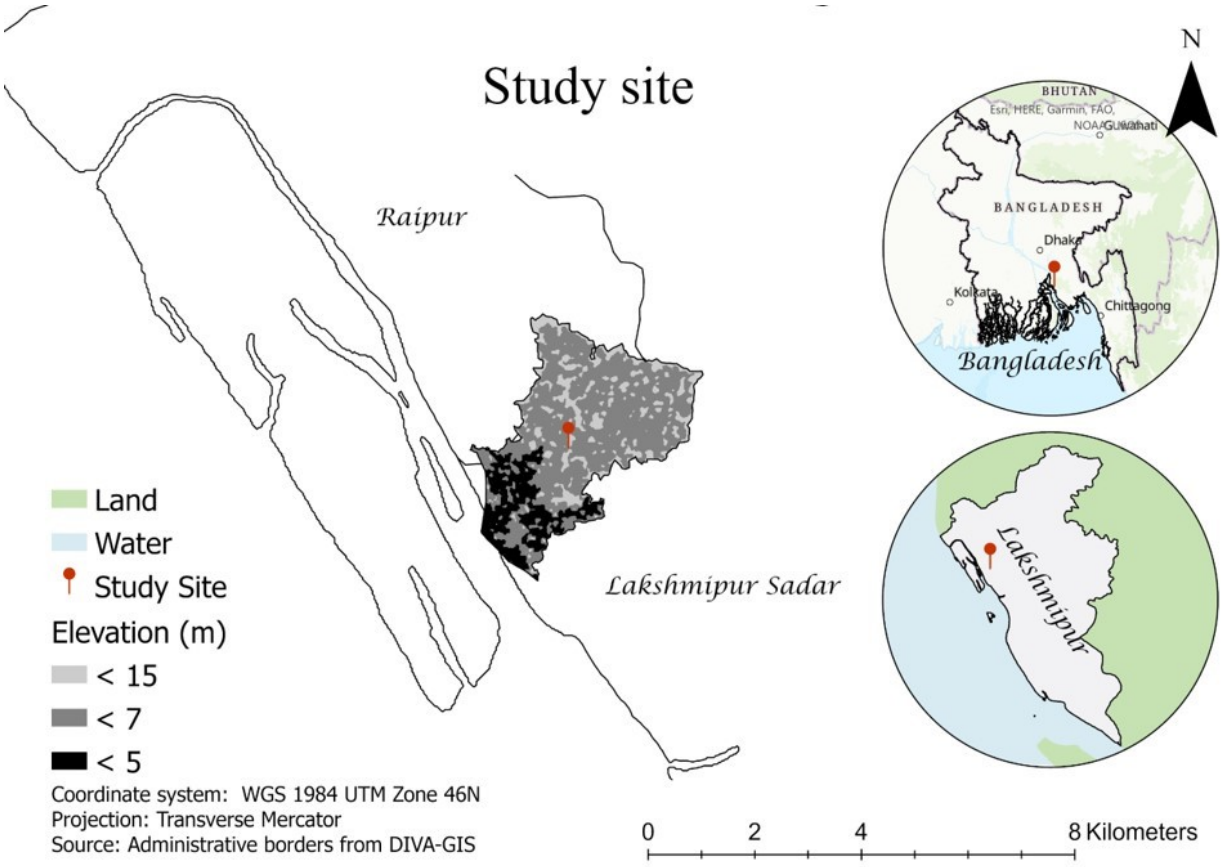

Figure 1. The study site in relation to some administrative areas in Bangladesh. The catchment is situated in the Lakshmipur district, located in south central Bangladesh. The catchment is situated across two upazilas, municipalities, Raipur and Lakshmipur Sadar.

3.2 Shared socioeconomic pathways

The first contribution of the 6th Assessment Report by the IPCC was issued in 2021 and it introduced the SSP framework for projecting future climate. The framework is based on the previous Representative Concentration Pathway (RCP) scenarios but additionally incorporates socioeconomic and political development for climate adaptation and mitigation (Riahi et al., 2017). The scenarios SSP2-4.5, SSP3-7.0, and SSP5-8.5 represent the emission scenarios intermediate, high, and very high respectively, and they resemble the radiative forcing for the corresponding RCP scenarios. SSP2 represents a middle of the road scenario where historical socio-economic trends remain unchanged, SSP3 a rocky road scenario with increasing inequalities and nationalism, and SSP5 a highway scenario with rapid increase in energy use and economic growth. All socioeconomic narratives along with the corresponding radiative forcing and greenhouse emissions are outlined in Riahi et al. (2017). Climate projections were generated through the Coupled Model Intercomparison Project (CMIP) Phase 6, which combines results from various general circulation models (GCM) into one multi-model ensemble.

3.3 Data acquisition and processing

All data were clipped to the study area and projected into the coordinate system WGS 1984 UTM Zone 46N with datum WGS 1984 and the projection Transverse Mercator. All raster data were harmonized into a horizontal resolution of 10 m and vertical resolution in decimetres.

The data processing and analysis in section 3.6.2-3.6.5 and 3.7.2 and creation of maps were completed using ArcGIS Pro 2.7.0 software by Esri (Environmental Systems Research Institute,

2020), and Microsoft Excel 2019 version 16.3 was used for processing and analysis of the data in Sections 3.5, 3.6.1, and 3.7.1. Flood modelling was performed using the TFM-DYN algorithm (Nilsson et al., 2021; Pilesjö & Hasan, 2014). All downloaded data and variables with their corresponding sources are outlined in Table 1, and their geographical locations are shown in Figure 2.

Table 1. Used data sets, the variable they were used to generate or represent, the section where processing and analysis of the variable is described, along with the corresponding sources.

Data set	Variable	Description	Source
Average largest 1-day precipitation	Extreme Precipitation	Section 3.5.2	(CCKP, 2021)
Average monthly precipitation	Mean precipitation	Section 3.5.2	(CCKP, 2021)
Historical daily rainfall	Mean precipitation	Section 3.5.2	(Bangladesh Meteorological Department, 2016)
Hourly tide gauge data	Tidal contribution	Section 3.6.1	(Caldwell et al., 2015)
SRTM 1-Arc Second Global V3	Topography	Section 3.6.2	(NASA JPL, 2013)
Sentinel-2B L2A	Land cover	Section 3.6.3	(European Space Agency, 2020)
Google Earth imagery	Land cover	Section 3.6.3	(Google, 2022)
Infiltration rate	Infiltration	Section 3.6.4	(Brouwer et al., 1990)
Manning's n values	Surface roughness	Section 3.6.5	(Mattocks & Forbes, 2008; Papaioannou et al., 2018)
Sea level rise	Sea level rise	Section 3.7.1	(Gutiérrez et al., 2021; Iturbide et al., 2021)
Regional subsidence rate	Land subsidence	Section 3.7.1	(Becker et al., 2020)
Global Surface Water	Evaluation	Section 5.1	(Pekel et al., 2016)
Coastal Aqueduct Flood Hazard Maps	Evaluation	Section 5.1	(World Resources Institute [WRI], 2020)

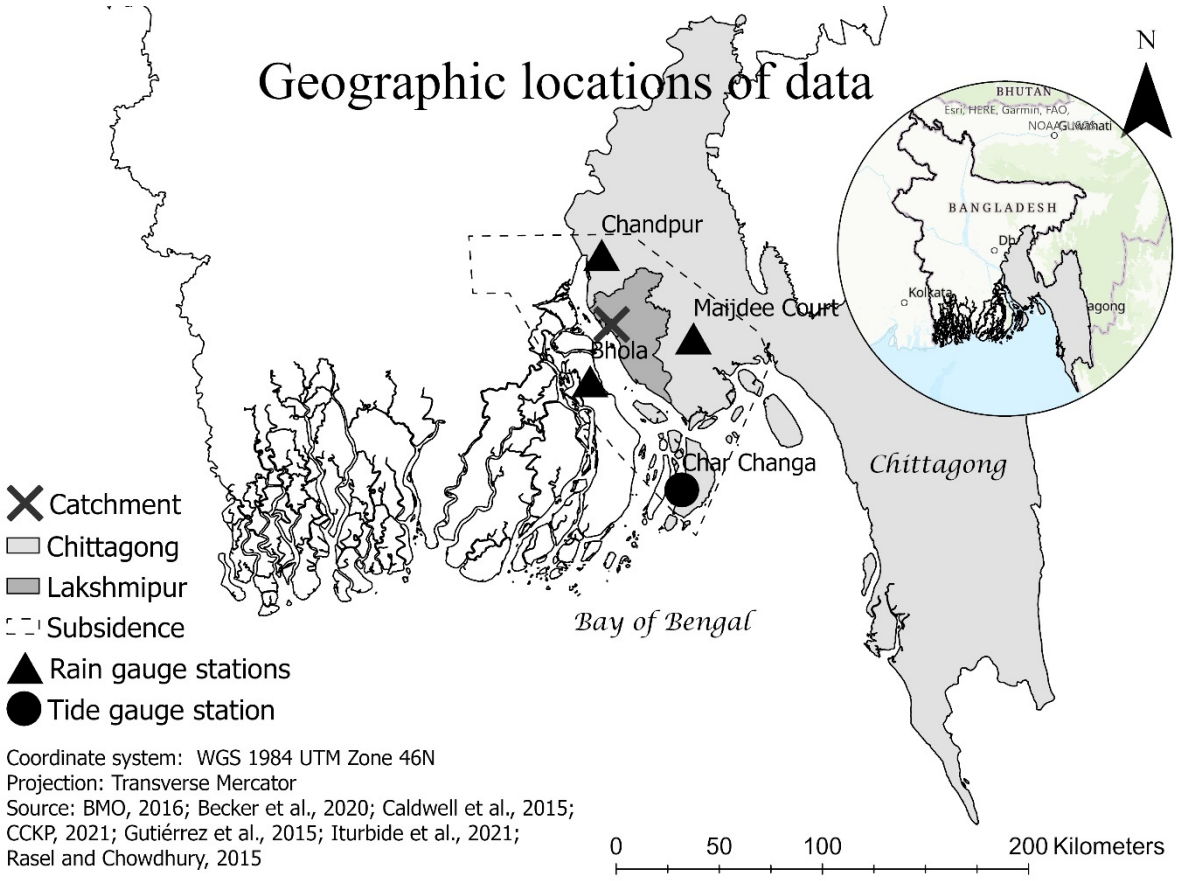

Figure 2. Geographic location of stations and areas where data were retrieved. Precipitation data was retrieved for the division Chittagong, sea level rise for the Bay of Bengal, rain gauge data from three stations surrounding Lakshmipur, tide gauge data from Char Changa, and subsidence for the GBM floodplain.

3.4 TFM-DYN

3.4.1 TFM algorithm and model

The triangular form-based multiple flow algorithm (TFM), created by Pilesjö & Hasan (2014), is an algorithm for accurately estimating overland flow and accumulation across a digital elevation model (DEM). It simulates flow distribution based on different hydrological processes and is a suitable approach since it provides an overall more accurate representation of water flow than other eight commonly used flow algorithms (Pilesjö & Hasan, 2014). One advantage of the algorithm is that flow direction is estimated by dividing each cell in a DEM into eight triangular facets, which allows water to flow into one or more neighbouring cells depending on the slope and aspect of each facet.

The TFM algorithm has additionally been developed into a user-friendly model by Nilsson et al. (2021), where water depths, volumes, and velocities are simulated throughout and after a precipitation event. It allows for temporally and spatially varying precipitation intensity, infiltration rates, and surface roughness as input, together with a DEM and optional inlets and outlets. For each time step in the model, precipitation depth is first added to each cell, then distributed to neighbouring cells according to the TFM algorithm, and lastly the current water depth is reduced according to the infiltration rate. Outputs can be saved in different time steps, and processing of data and results can be done using GIS software.

3.4.2 Simulation setup

Eight simulations were conducted using TFM-DYN and a detailed simulation setup is presented in Appendix B. One mean and one extreme event was simulated for each of the scenarios SSP2, SSP3, and SSP5, as well as for the 2010 baseline simulation. Each precipitation event was set to 12 hours with 30-minute intervals on the assumption that a total daily rainfall could occur in that time. The total simulated time was 13 hours to allow water to accumulate and infiltrate for an extra hour after the rainfall stops.

3.5 Precipitation events

3.5.1 Rainfall intensity-frequency-distribution (IDF) equations

Since no sub-daily data on historical rainfall and future projections were available, spatially varying rainfalls events were created using rainfall IDF equations developed by Rasel & Chowdhury (2015). The use of rainfall IDF curves is a common approach in hydrological modelling for creating precipitation events (Dasgupta et al., 2015). IDF empirical equations (Equation 1) have been developed for precipitation events with different return periods using long-term precipitation data and are used to illustrate the relationship between rainfall intensity, duration of event, and the frequency of occurrence of a precipitation event (Rasel & Chowdhury, 2015).

$$i = x * (td)^{-y} \qquad (1)$$

Where i is rainfall intensity in mm/h, td is the duration of a rainfall in minutes, and x and y are fitted parameters that can be calculated based on analysis of long-term precipitation data for a specific region.

IDF equations can be used to prepare rainfall hyetographs through the alternating block method, an approach where rainfall intensity for a chosen duration peaks in the middle of the precipitation event and the remaining rainfall intensities are arranged in decreasing order (Na & Yoo, 2018). This method results in a design storm hyetograph where precipitation varies temporally in intensity and duration, which is the required input to TFM-DYN.

3.5.2 Estimating historical and future precipitation

The total daily rainfall for mean and extreme precipitation events were estimated for each scenario using regionally downscaled CMIP6 projections. The precipitation index largest 1-day precipitation (MX1day) was used to simulate an extreme event since it is commonly used to represent heavy precipitation events and high values correspond to high flood risks (CCKP, 2021). The available projections are averaged over the time period 2080-2099, where the largest 1-day precipitation for each year is combined into an average. Both historical data and future projections for July were retrieved from CCKP (2021) for the division Chittagong (Table 2).

Mean daily precipitation (MDP) was used to simulate the mean precipitation events. Since no daily projections were available from CMIP6, it was estimated by dividing mean monthly precipitation, which was available from CMIP6, for Chittagong in July with the average number of rainy days in July. Historical and future projections of monthly mean precipitation were retrieved from CCKP (2021) and daily rainfall data from Bangladesh Meteorological Department (2016). The average number of rainy days in July 1994-2014 was calculated using daily rainfall data for three neighbouring areas to Lakshmipur, where no data were available. The average of the three stations was used (Table 3), and a rainy day was defined by a minimum rainfall of 2.5 mm occurring in 24 hours (Nandargi & Mulye, 2012).

Table 2. Average largest 1-day precipitation (MX1day) and mean daily precipitation (MDP) in July in the region Chittagong. Units in mm per day. MX1day values were derived from CCKP (2021) and MDP estimated by dividing monthly average precipitation from CCKP (2021) with the average number of rainy days in July (Table 3).

	Baseline (1995-2014)	SSP2-4.5 (2080-2099)	SSP3-7.0 (2080-2099)	SSP5-8.5 (2080-2099)
MDP	19 mm	20 mm	21 mm	23 mm
MX1day	90 mm	108 mm	124 mm	170 mm

Table 3. Number of rainy days in July for three precipitation stations surrounding Lakshmipur.

	Bhola	Chandpur	Majidee Court
Average (1994-2013)	20	18	21

3.5.3 Precipitation input setup

Precipitation events for baseline and future scenarios were created using daily rainfall values (Table 2) and IDF parameters from Rasel & Chowdhury (2015). They constructed IDF parameters for each division of Bangladesh using daily precipitation data from 1974-2014 and by comparing two statistical approaches, of which the Gumbel probability distribution provided the highest correlation coefficient R. The Gumbel IDF parameters for the lowest return period of 2-years were derived for Chittagong.

Design hyetographs for each scenario were created from the IDF equation using the alternating block method. First, the rainfall intensities for a 12-hour rain with 30-minute intervals were calculated using Equation 1 and the Rasel & Chowdhury parameters. Second, the rainfall intensity for all intervals were altered by a factor to fit the historical and projected total daily rainfall (Table 2). Finally, hyetographs were created for all scenarios using the alternating block method and by assuming spatially homogeneous precipitation across the entire study site. The same distribution of rainfall intensities was applied to all scenarios. The mean and extreme hyetographs for both historic and future scenarios are shown in Figure 3 and 4.

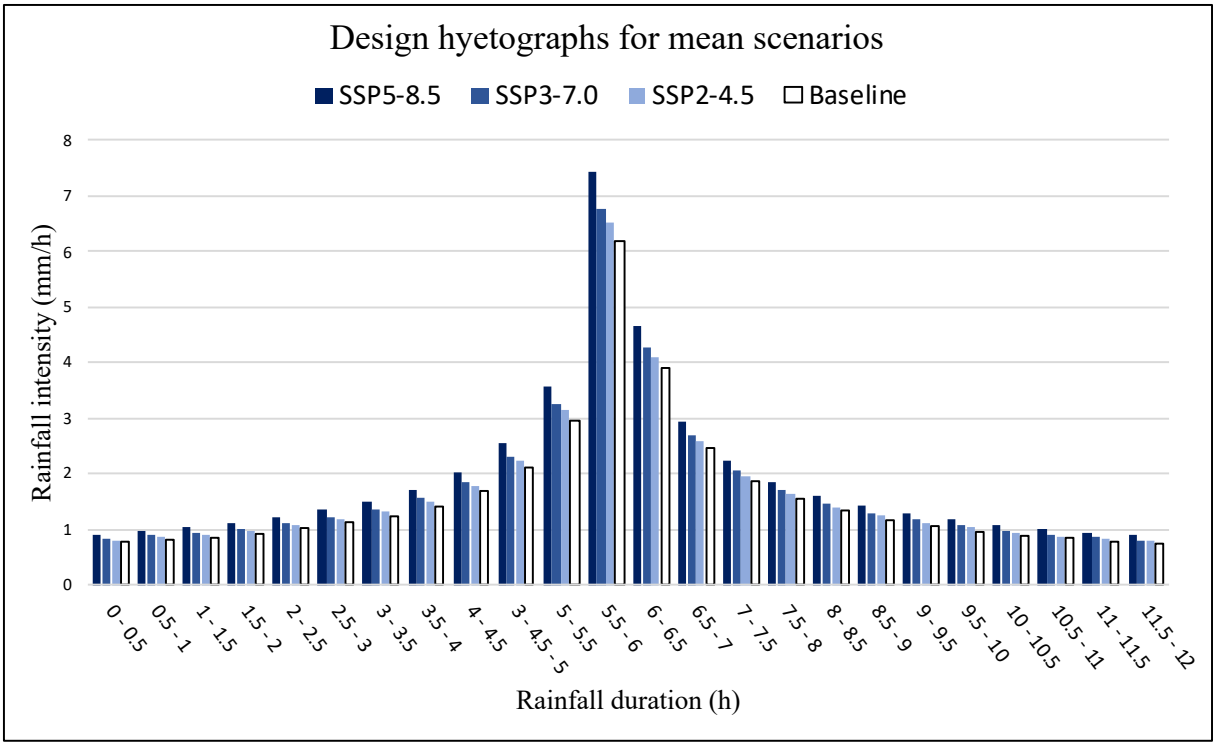

Figure 3. Design hyetographs for the mean scenarios showing rainfall intensities (y-axis) throughout the precipitation event in intervals of 30 min (x-axis). The 2010 baseline is presented in white and the SSP scenarios in blue, ranging from SSP2-4.5 in light blue, SSP3-7.0 in medium blue, to SSP5-8.5 in dark blue.

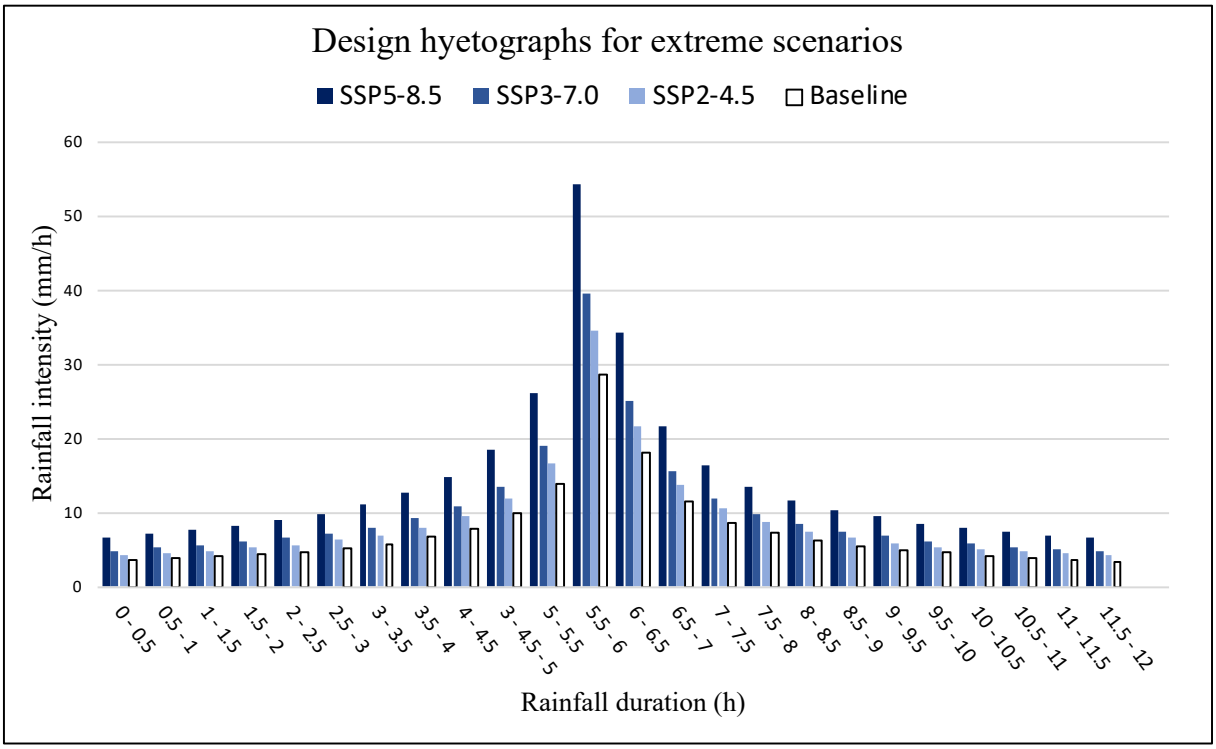

Figure 4. Design hyetographs for the extreme scenarios showing rainfall intensities (y-axis) throughout the precipitation event in intervals of 30 min (x-axis). The 2010 baseline is presented in white and the SSP scenarios in blue, ranging from SSP2-4.5 in light blue, SSP3-7.0 in medium blue, to SSP5-8.5 in dark blue.

3.6 Estimation of baseline landscape in 2010

3.6.1 Estimation of tidal contribution

The tidal pattern in the northern Bay of Bengal is semidiurnal and varies spatially along the coast. It increases towards the east, varying from 3 - 6 m along the central coastline (Nicholls et al., 2018). Many unprotected coastlines are easily flooded at high tide and correct estimations of local tidal influence is therefore important for flood modelling (Nicholls et al., 2018).

Hourly tide gauge data were used to estimate the difference in sea level between high tide and MSL. Hourly tide gauge data were retrieved from the University of Hawaii Sea Level Center, which offers research quality data of sea levels in millimetres for five stations in Bangladesh (Caldwell et al., 2015). The station Char Changa contains data from 1978-2000 with a data completeness of 96% and is the only station in central coastal Bangladesh and was thus used for analysis. First, daily maximum and daily average sea level were computed for each day in July 1978-2000. Second, the difference between daily maximum and daily average were computed. Finally, the greatest difference between daily maximum and daily average for each year were combined into an average for the period 1978-2000 (Appendix A).

3.6.2 Topography

Accurate modelling of water flow and accumulation requires a high-resolution DEM that realistically represents elevation features of a landscape. The highest resolution available for free in Bangladesh is 1-arc second (~30 m), provided by ASTER and Shuttle Radar Topography Mission (SRTM). The latter was chosen due to its higher vertical and horizontal accuracy which locally has been confirmed to be even higher and more suitable for Bangladesh (Rabby et al., 2020; Yao et al., 2020). The DEM was acquired in February 2000, has a vertical resolution of 1 m, horizontal accuracy of 20 m, vertical accuracy of 16 m, and the vertical datum is MSL (Earth Resources Observation and Science Center, 2018; Elkhrachy, 2018; Smith-Konter & Sandwell, 2003).

SRTM 1-Arc Second Global tiles covering the study area were retrieved from USGS Earth Explorer (NASA JPL, 2013). They were mosaiced into a new raster and sinks were filled as suggested in Shamsudduha et al. (2008), using tools available in ArcGIS. Even considering the limitations of the low resolution which is not a realistic representation of the true elevation, it was the best available elevation data and was thereby used in the analysis. The DEM was instead interpolated into a higher resolution by conversion from integer to float and interpolation into a horizontal resolution of 10 m using a bilinear algorithm (Esri, 2022). The bilinear algorithm calculates the value of each cell by averaging the values of the surrounding four cells which are weighted by distance, and it is recommended for continuous data. This allowed the DEM to store elevation in decimetres with higher resolution which fits the vertical resolution of relative SLR and tidal influence better. However, the accuracy and resolution of the DEM is still low, and results must be carefully assessed.

The DEM was modified according to the high tide contribution to simulate the current coastline at high tide. No modifications were applied to account for coastline change between 2000 and 2010 since relative SLR during that period is estimated to be less than one decimetre.

3.6.3 Land cover

Land cover data is required to estimate spatially varying infiltration and surface roughness values. Due to the low resolution of the available land cover data sets, land cover was digitized manually in ArcGIS Pro using a Sentinel-2 satellite image and a georeferenced Google Earth Pro image (Figure 5).

A Sentinel-2 image with 10 m horizontal resolution was retrieved from the Copernicus Open Access Hub (European Space Agency, n.d.). The available satellite images of the study area

were sensed between 2018-2022 and few cloud-free images were available from May-October. An image captured on April 1, 2020, was downloaded since it contained no cloud cover and was sensed from the nearest possible date to July. A high-resolution Google Earth Pro image was additionally downloaded and georeferenced to the Sentinel-2 image using 31 ground control points and a 2nd order polynomial transformation which provided the best root mean square error (RMSE), 4.57 m, even considering the possible extrapolation error (Google, n.d.). The image was provided by Airbus, who offer multispectral satellite data with horizontal resolutions between 2-6 m (Sentinel Hub, n.d.). The image was captured on November 21, 2017 and was the best available image considering no cloud cover to occur, time of capture to be close to July, and it being easy to distinguish features in the landscape.

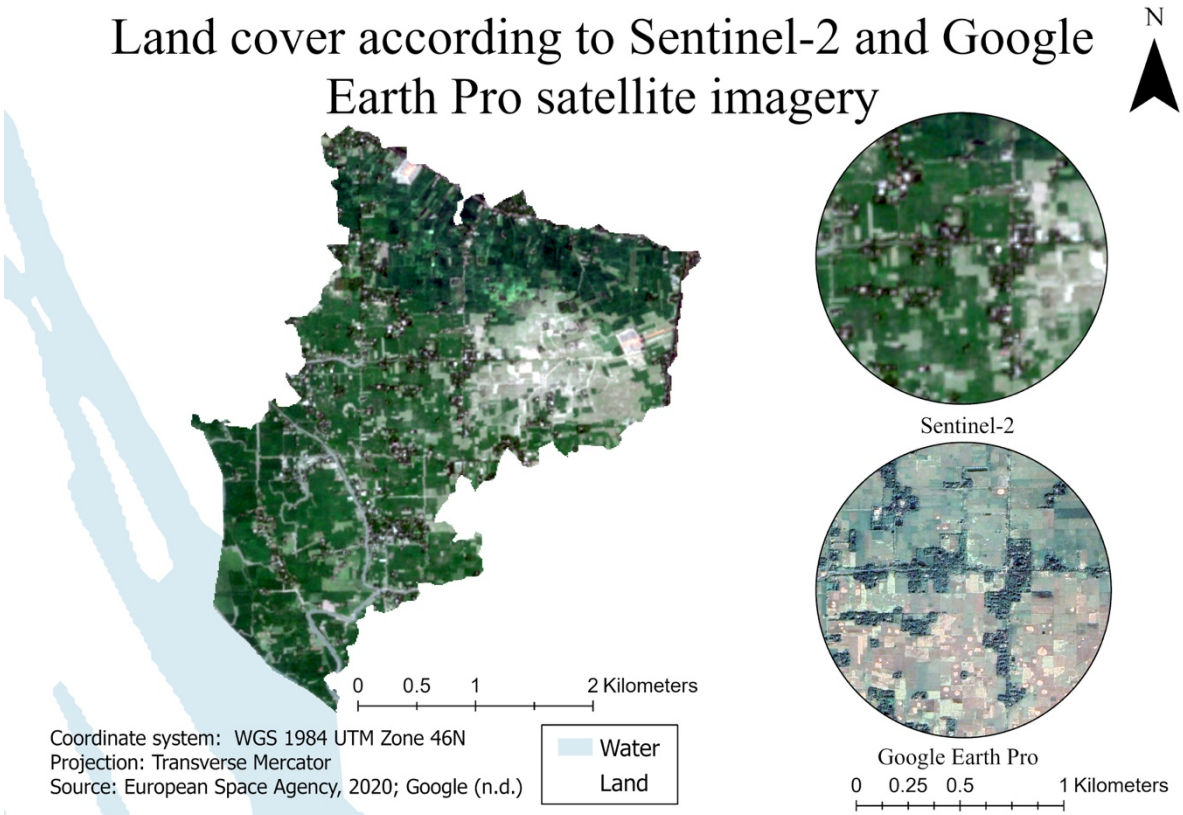

Figure 5. Satellite imagery from Sentinel-2 covering the study area to the left, and a detailed area in the central study site according to satellite imagery from Sentinel-2 (above) and Google Earth Pro (below) to the right. The horizontal resolution of Sentinel-2 is 10 m, and the Google Earth Pro image has a horizontal resolution between 2-6 m. The landscape is highly agricultural with the exception of smaller areas occupied by trees and shrubs. Water is visualised in blue and land in white.

3.6.4 Infiltration

Soil infiltration capacity varies depending on soil characteristics such as texture and grain size distribution, the hydrological condition of the soil as well as vegetation cover (Pingping et al., 2013). The soils in central coastal Bangladesh are extensively influenced by weathered alluvial deposits in the delta, are loamy in texture and contain 40-45% clay that is constant with depth (Huq & Shoaib, 2013). The dominant soils in Lakshmipur are ferric acrisols (FAO, 2003).

The infiltration rate of 10 mm/h for clay loams was retrieved from an FAO report by Brouwer et al. (1990). Soil infiltration decreases with increasing vegetation cover as a result of interception evaporation and changes in physical and chemical soil properties with the accumulation of organic matter in the soil (Pingping et al., 2013). The bare soil infiltration rate was used for croplands since rice harvesting and replanting of crops occur in July and August,

and very little vegetation cover is expected to occur to influence canopy interception (Shelley et al., 2016). Previous studies present rainfall interception rates of 20-60% for deciduous tree species, which are likely to be overestimated, and the resulting decrease in soil infiltration generally is higher than the interception rate (Wang et al., 2017; Yang et al., 2019). To account for the uncertainties, the infiltration rate for bare soil was decreased by 20% for deciduous tree cover and 10% for mosaic tree and shrub. A raster with spatially distributed infiltration rates according to land cover (Table 4) was created.

Table 4. Soil infiltration rate for each land cover class in the study area derived based on data from Brouwer et al. (1990) and information from Shelley et al. (2016), Yang et al. (2019) and Wang et al. (2017).

Land cover class	Infiltration rate (mm/h)
Cropland	10
Deciduous tree cover	8
Mosaic tree and shrub	9
Water bodies	0

3.6.5 Surface roughness

Surface roughness represents the resistance to water flow and varies spatially across a landscape due to differences in factors such as land cover and vegetation (Mattocks & Forbes, 2008). The Manning's roughness coefficient is a commonly used variable for assigning surface roughness to land use classes and can either be calculated using the Manning's formula or retrieved from various look-up tables (Mattocks & Forbes, 2008; Nilsson et al., 2021). Manning's coefficients for each land cover class were retrieved from look-up tables in Mattocks & Forbes (2008) and Papaioannou et al. (2018) and some Manning's coefficients were modified to adjust to the land cover in the study area. A raster with spatially distributed surface roughness according to land cover was created (Table 5).

Table 5. Manning's surface roughness coefficient for each land cover category in the study area derived from look-up tables in Mattocks & Forbes (2008) and Papaionnaou et al. (2018). The Manning's coefficient for mosaic tree and shrub was generated by combining deciduous tree cover and shrub into an average.

Land cover class	Manning's coefficient
Cropland	0.037
Deciduous tree cover	0.100
Mosaic tree and shrub	0.075
Water bodies	0.02

3.7 Estimation of future landscape by 2080

3.7.1 Projected relative sea level rise

Future projections of land subsidence and regional SLR were combined into relative SLR projections by 2080 for each scenario. Future regional SLR projections for the Bay of Bengal were derived from the IPCC WG1 Interactive Atlas (Gutiérrez et al., 2021; Iturbide et al., 2021). 50th percentile projections for 2081-2100 relative to 1995-2014 were used for the mean scenario

and 90th percentile projections for the extreme scenario. They were considered suitable to represent the change in 2080 due to the uncertainties in SLR projections. The regional land subsidence rate of 5.2 mm/year for central coastal Bangladesh presented by Becker et al. (2020) was used to project the total subsidence by 2080 relative to 2010.

3.7.2 Data modification according to coastline change

The DEM was modified according to projected relative SLR to simulate the resulting coastline change for each scenario at high tide. The coastline modification was achieved by a general GIS-based approach outlined in Anderson et al. (2018**)** and WRI (2020) where constant or spatially varying variables such as relative SLR and tidal influence can be incorporated to map coastal inundation extent using a passive flood mapping approach. First, the projected relative SLR was subtracted from the DEM for each scenario. Second, coastal areas with elevation below or equal to 0 were considered being submerged and new coastlines were extracted at these locations. Third, surface roughness and infiltration layers were clipped to the new coastlines.

4 Results

4.1 Tidal flooding

To assess future coastal areas flooded at high tide, a passive flood mapping approach was used to identify new coastlines considering the relative SLR in Table 6 and high tide to differ by 1.8 m from MSL.

Table 6. Total relative sea level rise and the contribution from SLR and land subsidence for each scenario. Sea level rise values were derived from the IPCC WG1 Interactive Atlas (Gutiérrez et al., 2021; Iturbide et al., 2021) and land subsidence calculated using data from Becker et al. (2020).

Scenario	Relative SLR (m)	Contribution from SLR (m)	Contribution from land subsidence (m)
SSP2-4.5 Mean	0.9	0.5	0.4
SSP3-7.0 Mean	1.0	0.6	0.4
SSP5-8.5 Mean	1.1	0.7	0.4
SSP2-4.5 Extreme	1.3	0.9	0.4
SSP3-7.0 Extreme	1.4	1.0	0.4
SSP5-8.5 Extreme	1.5	1.1	0.4

Figure 6 shows the coastlines for the baseline and future SSP scenarios at high tide. Coastline changes were observed in the south-eastern part of the catchment, whilst the eastern coastline was unaffected. Around 1% of the study area is seen to be inundated at high tide following the most extreme future relative SLR (Table 7). The greatest change in inundated area occurred for SSP5-8.5 for both mean and extreme scenarios, increasing by 25% and 48% respectively compared to the 2010 baseline (Table 7). The extreme scenarios resulted in a greater inundated area compared to the mean scenarios, and a larger difference between SSP scenarios was additionally observed. The inundated area ranged from 8.6-8.9 ha for the mean scenarios while ranging from 9.9-1.5 ha for the extreme scenarios, representing a change of 21-25% and 39-48% respectively (Table 7).

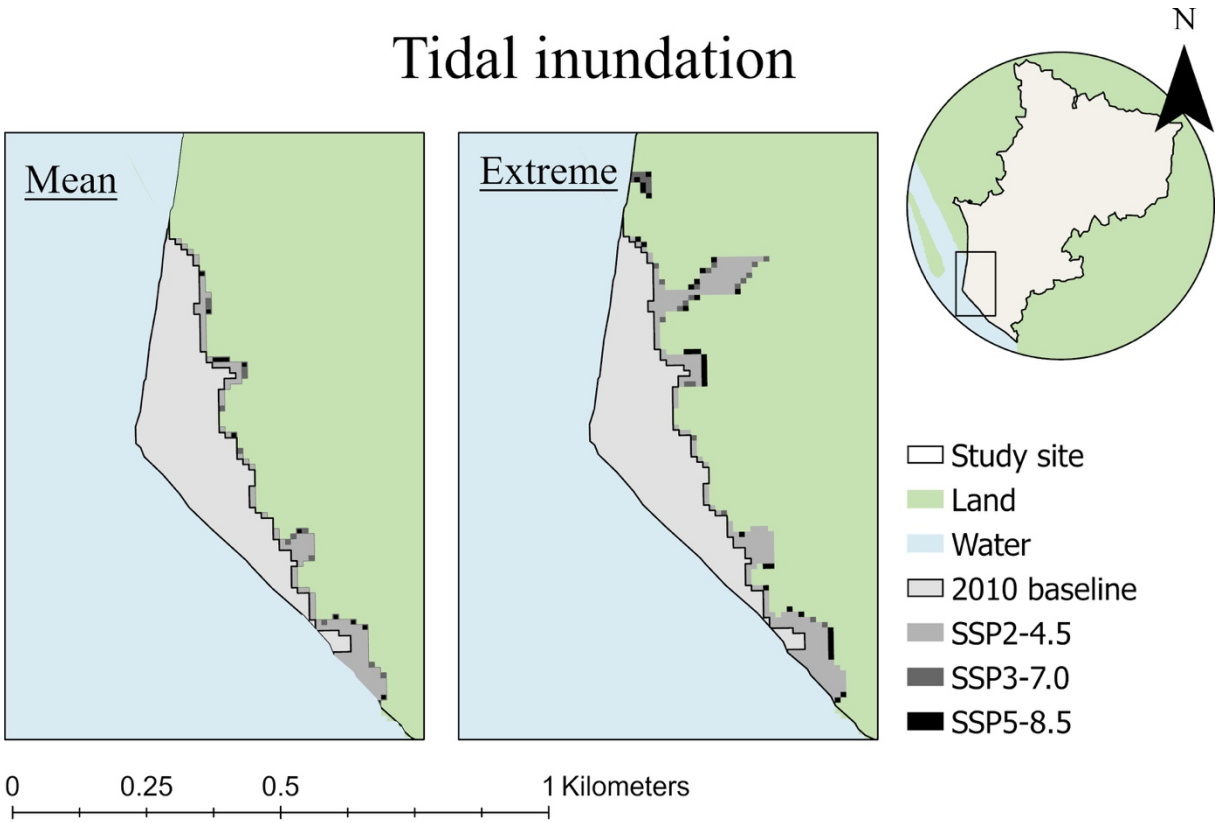

Coordinate system: WGS 1984 UTM Zone 46N
Projection: Transverse Mercator
Source: Becker et al., 2020; Caldwell et al., 2015; European Space Agency, 2020
Gutiérrez et al., 2021; Iturbide et al., 2021)

Figure 6. Tidal flooding for the 2010 baseline scenario (light grey), 2080 given SSP2-4.5 (medium grey), SSP3-7.0 (dark grey) and SSP8.5 (black) for mean scenario and extreme scenarios. Land is visualised in green, and water in blue.

Table 7. Area inundated at high tide by future relative sea level rise.

Scenario	Inundated area at high tide (ha)	Percentage of catchment (%)	Change from baseline (%)
Baseline	7.1	0.76	-
SSP2-4.5 Mean	8.6	0.92	+ 21
SSP3-7.0 Mean	8.7	0.93	+ 23
SSP5-8.5 Mean	8.9	0.95	+ 25
SSP2-4.5 Extreme	9.9	1.05	+ 39
SSP3-7.0 Extreme	10.1	1.08	+ 42
SSP5-8.5 Extreme	10.5	1.12	+ 48

4.2 Precipitation-induced flooding

The second set of analyses examined the change in flood extent and depth with future precipitation events using TFM-DYN. A flooded area is defined as flood depths above 0.1 m as suggested by previous flood studies conducted in Bangladesh (Dasgupta et al., 2010; Dasgupta et al., 2015).

Table 8 presents the flood extent for the 2010 baseline scenarios. There is a trend of increasing flood extent throughout and after the rainfall for both mean and extreme scenarios,

and greater flood extent was observed for the extreme scenario (Table 8). Figure 7 compares the change in flood extent by 2080 across mean and extreme scenarios. Although a higher magnitude of change is observed for the extreme scenarios (Figure 7b), both follow a similar trend of increasing flood extent across all SSP scenarios that gradually decreases with time. Almost no change in flood extent is observed after the rainfall for the mean scenarios (< 1%). The greatest change in flood extent occurs at mid rainfall across both mean and extreme scenarios. Change in flood extent remains constant between end of rainfall and one hour after rainfall for mean SSP2-4.5 and SSP3-7.0 (Figure 7a), whilst it decreases across the extreme scenarios. The trend of flood extent increasing with time that was observed for the baseline scenarios (Table 8) remains across all future scenarios.

Table 8. Flood extent throughout the precipitation events for 2010 baseline scenario. Flood extent includes areas with water depths greater than 0.1 m. The flood extent for mid rainfall (6 hours), end of rainfall (12 hours), and one hour after rainfall (13 hours).

Time	Mean scenario (ha)	Percentage of catchment (%)	Extreme scenario (ha)	Percentage of catchment (%)
6h	286.4	30.6	337.6	36.1
12h	348.8	37.3	392.9	42.0
13h	354.7	37.9	396.2	42.3

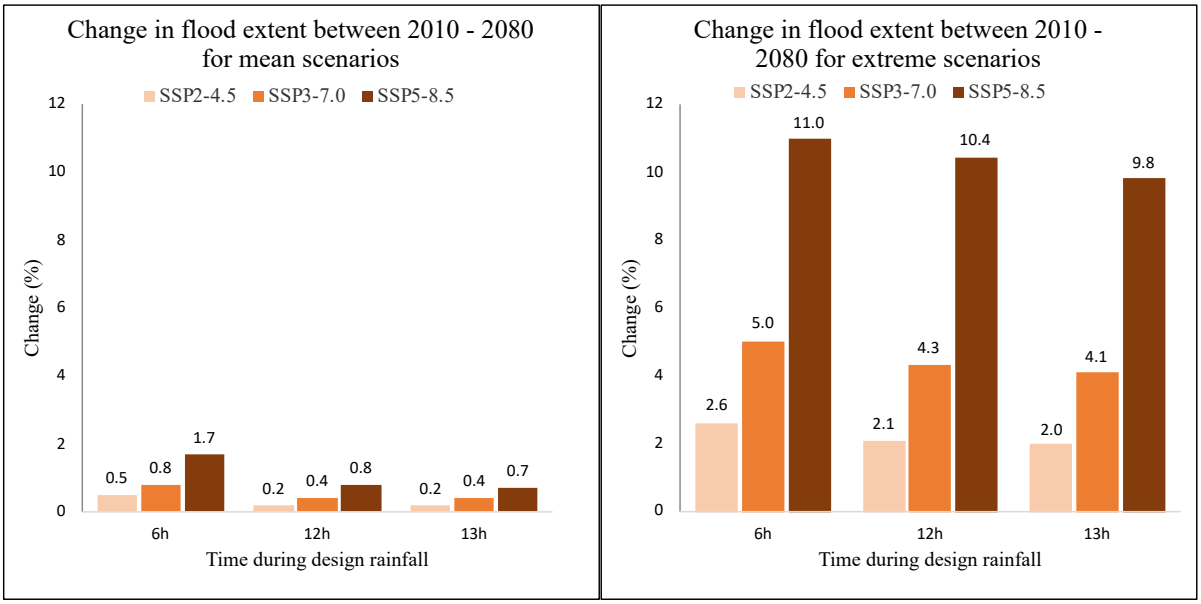

Figure 7. Change in flood extent throughout the precipitation by 2080 relative to 2010 for a) mean scenarios and b) extreme scenarios. The change in percent (y-axis) is visualized for each SSP scenario for mid rainfall (6 hours), end of rainfall (12 hours), and one hour after rainfall (13 hours).

Figures 8 and 9 show flood depths for selected areas according to the lower and upper SSP scenario one hour after rainfall. It can be observed how water extent and depth changes depending on the scenario applied, compared to baseline scenarios. The map shows areas where the highest water depths are found, the northwest and central (Figure 8) and central east (Figure 9). The highest water depths are observed for SSP5-8.5, which is followed by the extreme baseline scenario. Interestingly, little change is observed between the flood depth pattern for mean baseline and mean SSP2-4.5.

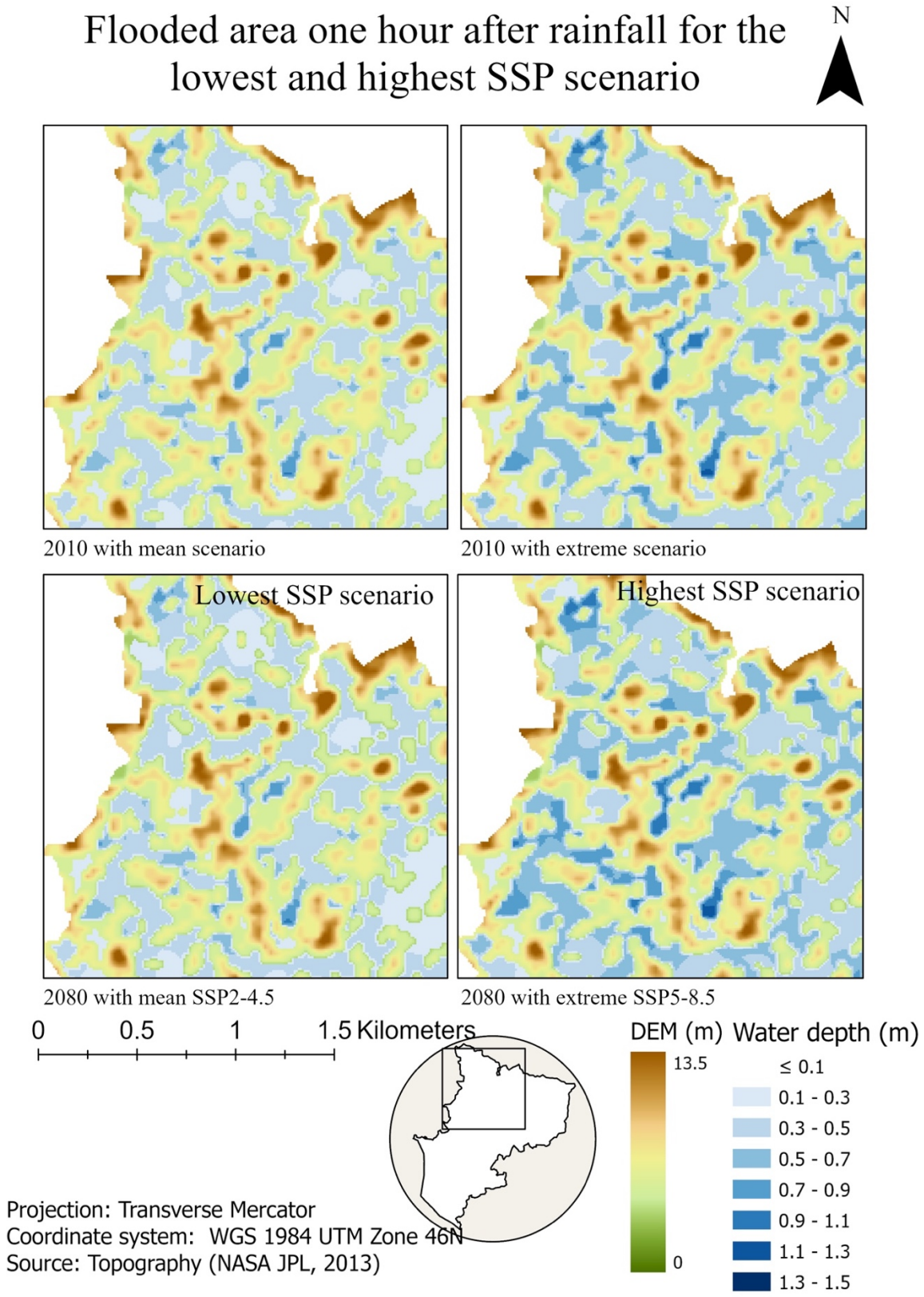

Figure 8. Flooded areas for baseline scenarios (above) and the highest and lowest SSP scenarios (below) one hour after rainfall (13 hours). The lowest SSP scenario refers to mean SSP2-4.5, and the highest scenario refers to extreme SSP5-8.5. Flood depths are visualized on top of a DEM, ranging from low elevations (green) to high elevations (red) and the white areas are located outside of the study area.

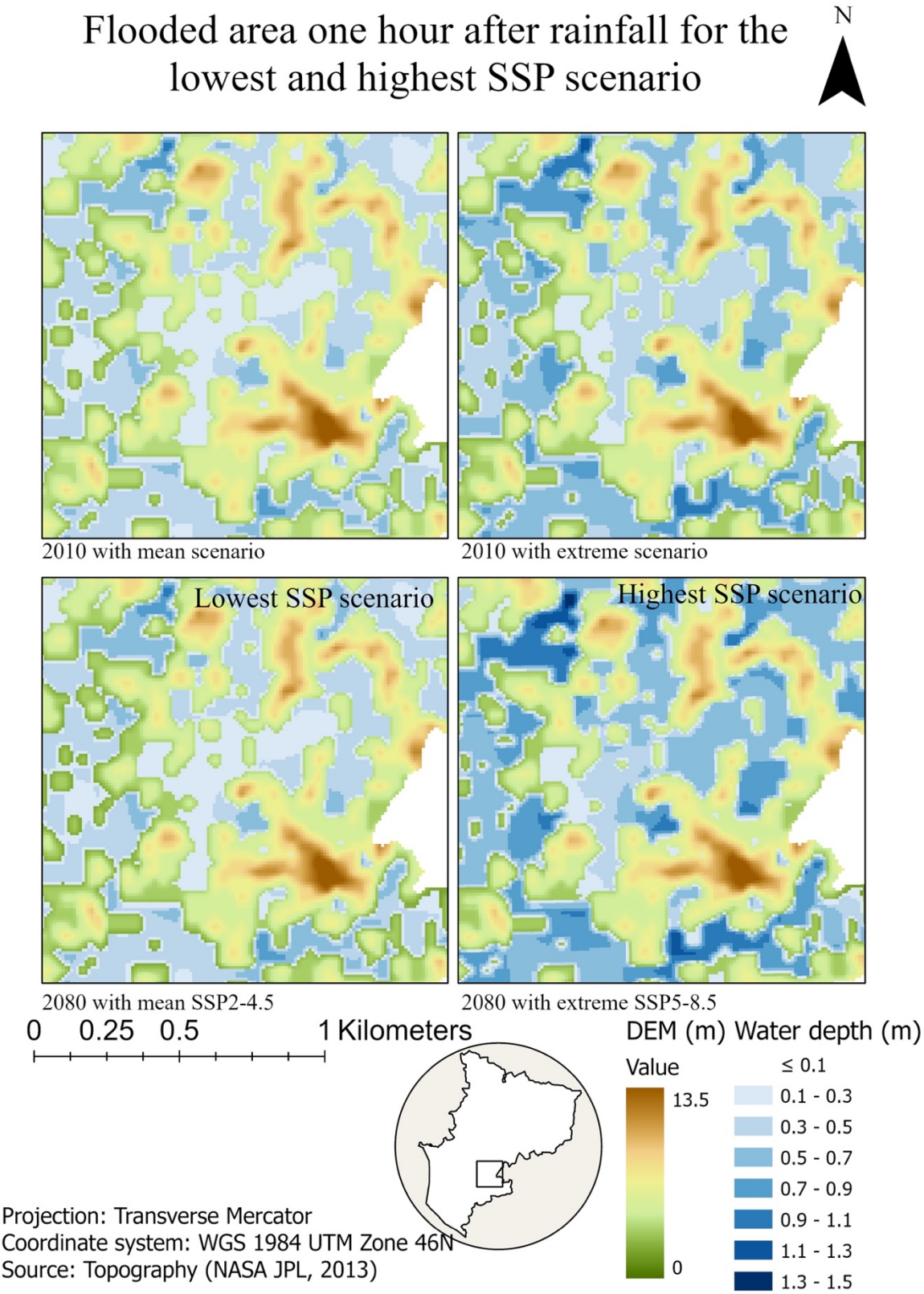

Figure 9. Flooded areas for baseline scenarios (above) and the highest and lowest SSP scenarios (below) one hour after rainfall (13 hours). The lowest SSP scenario refers to mean SSP2-4.5, and the highest scenario refers to extreme SSP5-8.5. Food depths are visualized on top of a DEM, ranging from low elevations (green) to high elevations (red), and the white areas are located outside of the study area.

Figure 10 shows the change in inundated area per flood depth one hour after rainfall relative to 2010. From the baseline data in Table 9, greater areas are occupied with higher flood depths above 0.5 m for the extreme scenarios compared to the mean. A decrease of inundated areas with low depths and increase of areas with high depths can be observed for the future scenarios, with higher decrease occurring for the extreme scenarios (Figure 10). Whilst water depths up to 0.3 m decrease in area for the mean scenarios (Figure 10a), depths up to 0.5 m decrease for the extreme scenarios (Figure 10b). Interestingly, the higher the SSP scenario, the higher the magnitude of change in both reduction and increase. Even though the mean and extreme events follow a similar pattern, the magnitude of change is much larger for the extreme events, which also reach higher absolute depths.

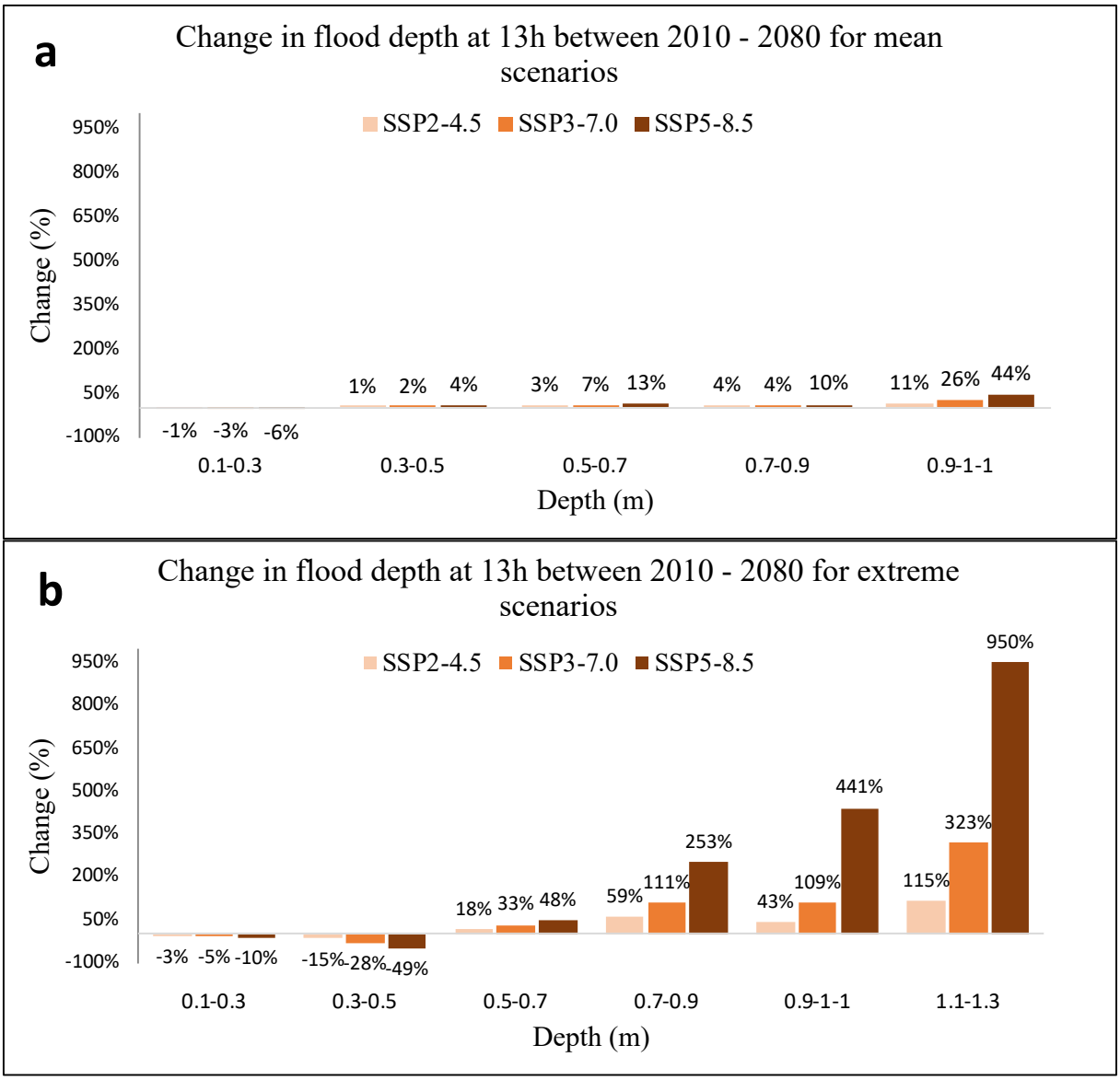

Figure 10. Change in inundated area per depth one hour after rainfall by 2080 relative to 2010 for a) mean events and b) extreme events.

Table 9. Inundated area per flood depth for 2010 baseline scenarios one hour after rainfall. The total catchment area is 936 ha.

Inundation depth (m)	Mean scenario (ha)	Extreme scenario (ha)
0.1 - 0.3	143.9	82.7
0.3 - 0.5	176.5	171.2
0.5 - 0.7	30.7	115.4
0.7 - 0.9	3.4	23.2
0.9 - 1.1	0.3	3.5
1-1 - 1.3	0.0	0.3

Figure 11 compares the inundated area per flood depth by 2080 to the 2010 baseline given extreme SSP scenarios one hour after rainfall when the highest flood extent occurs. Not only does the SSP5-8.5 scenarios result in the highest magnitude of change, but it also results in water depths that cannot be observed for other scenarios. Table 10 presents the inundated area per flood depth at the end of rainfall. By comparing it with Figure 11, it is apparent that water depths below 0.5 m occupy a larger area by the end of rainfall, and that water depths above 0.5 m occupy a larger area one hour after the rainfall. This is visualized in Figure 12, where flood depth throughout the extreme SSP5-8.5 rain is visualized on topography data. Water is seen accumulating at lower elevations, and the areas with high water depths are increasing throughout and after the rain (Figure 12).

Flood depth maps for all means and extreme scenarios are available in Appendix C. As previously stated, little change in flood depth and extent can be observed for mean SSP scenarios. Tables with values for flood extent and flood depth are additionally available in Appendix D.

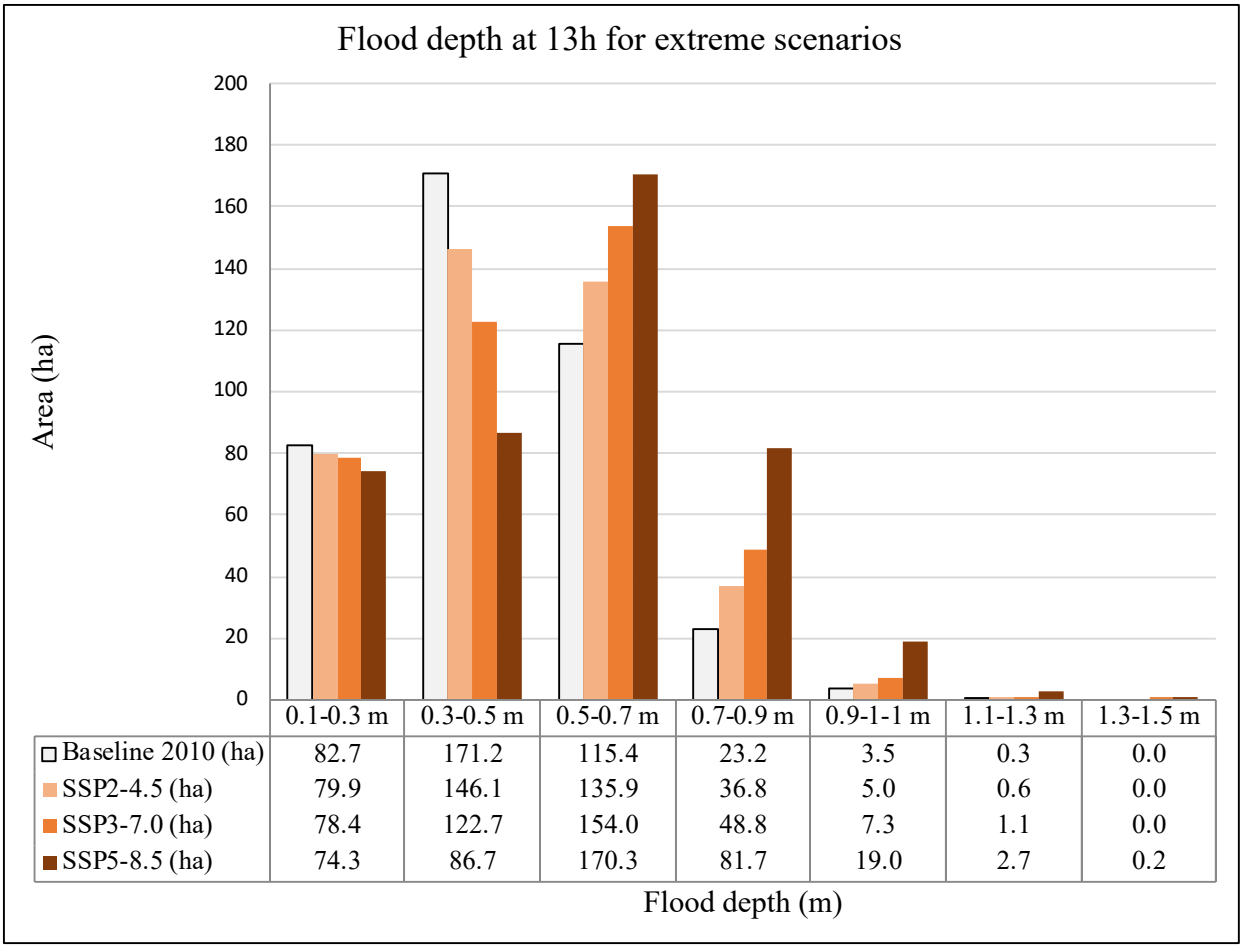

Figure 11. Inundated area per flood depths at end of rainfall (13 hours) for all extreme scenarios. The bar chart above shows the area (y-axis) inundated per flood depth (x-axis). The table below compares the inundated area for each depth.

Table 10. Inundated area per flood depth in ha at end of rainfall (12h) for all extreme scenarios.

	0.1-0.3 (m)	0.3-0.5 (m)	0.5-0.7 (m)	0.7-0.9 (m)	0.9-1.1 (m)	1.1-1.3 (m)	1.3-1.5 (m)
Baseline (ha)	85.1	187.1	99.4	18.3	2.9	0.1	0.0
SSP2-4.5 (ha)	81.5	163.4	122.9	28.9	4.1	0.4	0.0
SSP3-7.0 (ha)	79.9	141.9	141.2	40.4	5.6	0.8	0.0
SSP5-8.5 (ha)	75.9	92.9	173.9	72.7	15.9	2.2	0.1

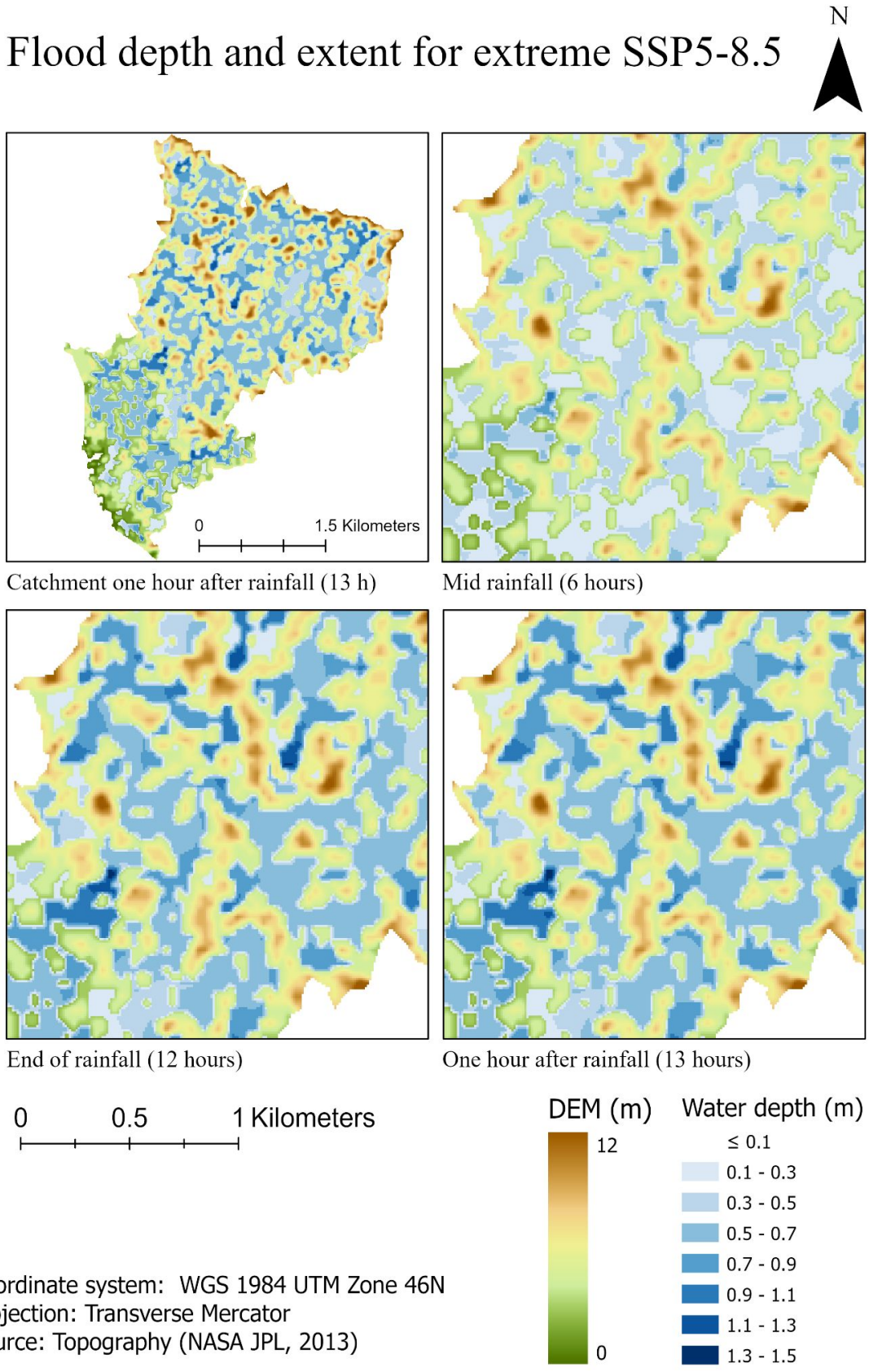

Figure 12. Flood depths and extent throughout and after the extreme SSP5-8.5 rainfall. Water depths are visualized ranging from light blue to dark blue on top of elevation data from low elevations (green) to high elevation (red). Areas in white are outside of the study site.

5 Discussion

5.1 Tidal flood analysis

One objective of the study was to assess the change in coastal flood extent by 2080 at high tide following future projections of relative SLR. One interesting finding is how change in flood extent ranges from 21-48 % between the lower and upper scenario, mean SSP2-4.5 and extreme SSP5-8.5. Even though all scenarios resulted in an increase in flood extent, these results highlight how the uncertainties with SLR translates to how the area exposed flooding could increase up to 50% with extreme SSP5-8.5 compared to 2010. The study found the flood extent to increase by 39-48% for extreme scenarios and 21-25% for mean scenarios, however the extreme scenarios of SLR, the 90th percentile projections, are more unlikely to occur compared to the mean, 50th percentile projections. That being said, extreme scenarios should not be ruled out considering the uncertainties with glaciers and ice-sheet dynamics in GCMs and possible compound effects such as storm surge, tropical cyclones, and waves (IPCC, 2021). Surprisingly, little change in inundation extent occurred between each SSP scenario for mean and extreme events, respectively. This is however likely considering the relative SLR differed by 0.1 m between each SSP scenario. Additionally, it could be because the increments of relative SLR being too small to have an impact on the elevation data, originally having coarse vertical resolution. Again, considering the uncertainties with SLR projections, the range of increase in inundation extent across all projections is more relevant than scenario specific results.

The results can be compared with the water occurrence and water recurrence data sets from Global Surface Water, which are based on satellite observations of surface water presence during a certain period (Pekel et al., 2016). In short, occurrence represents annual water occurrence between 1984-2020 and recurrence the seasonal behaviour of water and the frequency with which water returns every year. The recurrence data set confirms that the mapped inundated area at high tide for the baseline scenario regularly is inundated seasonally, which confirms the findings for the baseline scenario. The occurrence and recurrence data sets both map the areas subject to become inundated by 2080 (Figure 4) as historically inundated at time, which is likely considering occasional inundation by high river discharge, extreme tides, storm surge, and tropical cyclones. This confirms that these areas are vulnerable to ocean-related hazards, and that the extent of inundation from ocean-related hazards additionally is likely to move further inland with future coastline change.

The results can additionally be compared with 1-year flooding depths for historical 2010 and future 2080 from the Global Aqueduct Coastal Flooding data set (WRI, 2020). WRI provides projected global coastal inundation given SSP2-4.5 and SSP3-7.0 for various return periods and incorporates mean and extreme SLR (50th percentile and 95th percentile), land subsidence, storm surge, and tide. The inundation depths across all scenarios are higher compared to the findings in this study, which is expected considering it incorporates storm surges from tropical cyclones. Flood depth increases with higher SSP scenarios and extreme SLR, with depths ranging between 0.6-1.1 m in 2010, 1.2-3.4 m by 2080 with SSP2-4.5, and 1.3-3.6 m by 2080 for SSP3-7.0. The tidal inundation of 1.8 m used in this study falls into the range for all future scenarios and can thereby be considered sound, however it is not possible to confirm whether the tidal inundation depth is underestimated or overestimated.

5.2 Precipitation-induced flood analysis

The study additionally assessed the change in flood extent and depth of precipitation-induced floods. For all scenarios, the findings show that flood extent increases throughout the rainfall and culminates one hour after the rain stops. The highest change in flood extent for the extreme

scenarios is however observed at mid rainfall, indicating that higher flood extent could occur earlier in a rainfall in the future. Flood extent increases up to 9.8% for the extreme scenarios, which could result in a greater population being exposed to flooding. The low change in flood extent observed for mean scenarios (< 1%) is however unlikely to have any significant impact on the population. These results are supported by the findings in Dasgupta et al. (2010), where a small increase of 4% in flood extent was observed on a national scale for Bangladesh by 2050 under SRES A2, which resembles SSP3-7.0.

Flood depths are shown to increase in magnitude with higher rainfall, and observations of water depths up to 1.5 m were found for the extreme SSP5.8.5. Furthermore, higher amounts of rain results in greater areas occupied with deep water and less areas occupied with shallow water. These results support evidence from previous observations (Brown et al., 2018; Dasgupta et al., 2010). The highest water depths were additionally observed one hour after rainfall, which allows water to accumulate into higher water depths in the low-lying areas of the landscape. These results were especially noticeable for the extreme rainfalls, which aligns with historical observations of extreme rains posing a greater threat to the population (Dastagir, 2015). On the contrary, no noticeable change in flood depth was observed for daily mean rainfalls.

Water was mainly seen to accumulate in the depressions of the landscape, and no pattern was observed in terms of land cover due to the homogeneous nature of the study site. However, flooded areas are found throughout the landscape since the elevation is relatively homogenous. A high percentage of the area being flooded consequently results in damage to housing, crop yield, and infrastructure. These findings confirm that extreme rainfall events are a threat to the population in rural Bangladesh in the future, and that even higher water depths cannot be ruled out considering the historical daily extremes that have occurred.

According to the dataset Gridded Population of the World, the population density of Lakshmipur is above 1000/km^2 which corresponds to the highest population density class available in the dataset (Center for International Earth Science Information Network, 2018). By considering the population in Lakshmipur being greater than 1.7 million in 2011, which has increased since, and the size of the district being around 1440 km^2, the population density of the district is closer to 1200/km^2 (BBS, 2021). Considering both population densities, this indicates that the population exposed to flooding in the study area is estimated to 9000-11000 people. Given that the study site is representative of the neighbouring areas in central coastal Bangladesh, which also are mapped according to the same population density class, future extreme rainfall events has the potential to affect even a larger population.

5.3 Evaluation

Accurate high-quality ground data on flood extent and depth are rare and were not available for Bangladesh to use for the evaluation of the study results. The scarce information that exists on flood depth or extent from historical rainfalls are often the result of long seasonal monsoon rainfalls culminating in extreme daily rainfalls, and the flooding is additionally influenced by high river discharge from the heavy rainfall season. This data was not used due to time constraints of simulating long seasonal rainfalls and finding models to simulate riverine flooding. Additionally, the use of satellite imagery for detecting surface water in July was limited due to heavy cloud cover, which is persistent during July when the heaviest monsoon rainfalls occur. Cloud free satellite data or aerial photographs with high resolution would be required to identify local or regional flooding in detail to use for evaluation. A sensitivity analysis with the TFM-DYN input variables surface roughness, infiltration, and land cover could additionally have been performed to gain an understanding on the model performance in rural landscape in Bangladesh, but this was restricted due to time constraints. The evaluation of results was consequently limited to comparison with existing data sets. However, by

investigating the change between baseline and future flooding instead of absolute values, the lack of evaluation is not a strong limiting factor.

5.4 Errors and uncertainties

5.4.1 Method uncertainties

The passive flood mapping approach used for assessing coastal inundation is a simplified approach that does not fully incorporate all relevant processes for estimating coastline change. Although it is used for mapping and predicting future inundated areas in various reports and data sets, it has been proven to ignore some areas exposed to ocean-related inundation, such as tidal inundation with SLR projections, compared to complex hydrological models (Anderson et al., 2018). The level of uncertainty in the study site is however unclear, yet the missing effect of erosion and waves clearly underestimates the inundated area. To fully investigate coastline change, the use of complex models that include ocean and river dynamics should be used. The access to such models was however limited due to time constraints, and the extensive use of passive flood approaches was still considered sound to outline the vulnerable areas, even if underestimated.

Previous evaluation of the TFM-DYN algorithm should be highlighted in order to understand the accuracy of the resulting precipitation-induced flooding. The TFM algorithm was evaluated on four mathematical surfaces and the resulting flow direction and accumulation was compared with 8 commonly used flow algorithms (Pilesjö & Hasan, 2014). In terms of RMSE, it outperformed the others on three out of four surfaces, and was outcompeted by two algorithms on the plane surface. Additionally, no systematic bias was detected, and the flow accumulation can thereby be considered a sound approach to simulate flow in the study site. Subsurface water flow is not incorporated into the algorithm, and it is thereby not possible to quantify its impact on the results. The application of TFM-DYN to simulate precipitation-induced flooding was not evaluated to ground data due to the limited availability, yet a sensitivity analysis was performed using varying surface roughness (Nilsson et al., 2021). Nilsson et al. (2021) concluded that a decrease in surface roughness corresponds to a decrease in water depth and volume and increase in velocity. This implies that the precipitation-induced flooding could result in higher water depths if the surface roughness is underestimated.

5.4.2 Data uncertainties

The main uncertainties with the data revolve around the lack of regional high-quality data. Tidal contribution was assumed to be realistic by comparison with mean high tidal levels of 1.7 m south of the study site presented by Uddin Komol (2011) and considering the tidal range of central coastal Bangladesh. The use of Manning's roughness coefficients derived from look-up tables in research papers is additionally widely accepted in research and should thereby be sound for this study (Mattocks & Forbes, 2008; Nilsson et al., 2021; Papaioannou et al., 2018).

The resulting flood depth and extent will change depending on the chosen infiltration rates. The relatively low bare soil infiltration rate was derived from a general look-up table, however local infiltration rates would be required for accurately capturing the infiltration that varies with soil condition and texture. A similar conclusion can be drawn regarding the effect of canopy interception on soil infiltration, where regional studies would provide more accurate estimates to be used for analysis. However, waterlogging following long monsoon rainfalls or coastal flooding saturates the soils in coastal Bangladesh, which results in low infiltration rates occurring at times. The main uncertainty thereby regards the spatial variation between the land cover classes, and a possible underestimation. As the spatial variation in infiltration and surface roughness is based on land cover and soil data, high-resolution availability of these is additionally required for accurate parameterization, which was a limitation for Bangladesh.

One of the main limitations was the restricted availability of high resolution DEMs, which are crucial for accurate mapping of surface flow. Even by interpolating the DEM into a higher resolution, the precipitation-induced flood was still generated on a coarse DEM that does not capture the realistic flow accumulation perfectly. Assessing coastline change on global DEMs with vertical resolutions of 1 m additionally limits the accuracy of the results. There is a demand for improved elevation data sets with higher vertical and horizontal resolution for high confidence mapping of exposure to SLR and subsidence, especially for the low-lying areas of coastal Bangladesh that currently experience minor differences in elevation (Brown et al., 2018; Gesch, 2018). Whilst the demand remains, the currently accessible DEMs are still useful for general delineation of low future coastlines (Gesch, 2018).

Furthermore, future climate projections derived from global GCMs contain levels of uncertainty. First, the CMIP6 projections are downscaled results from combined global GCMs. Even though the CMIP project has the advantage of incorporating multiple models to account for differences in sensitivity and results, they might not capture the regional climate as well as regional climate models. As weather also varies locally, the regionally downscaled projections might even not be representative for smaller areas. Secondly, the future projections of precipitation patterns and SLR are some of the most difficult variables to simulate in future projections and are thereby influenced by large uncertainties (IPCC, 2021). Until GCMs can model glacier and ice sheet dynamics with higher confidence, SLR projections are uncertain.

Lastly, the difference in sea level between high tide and MSL is assumed constant up to 2080. This tidal contribution could however change in the future, for example with coastline alterations.

6 Conclusion

The aim of the study was to assess change in flood extent and depth from precipitation-induced flood and coastal tidal flooding by 2080 using future projections of rainfall and relative SLR. The four hypotheses were evaluated against the results.

i. The area inundated at high tide with future relative SLR increased across all scenarios compared to baseline. The greatest change was observed for SSP5-8.5 and the smallest for SSP2.4.5.
ii. Precipitation-induced flood extent and depth increased with higher SSP scenario. Higher water depths were observed, and the area inundated by high depths increased. The highest change was observed for SSP5-8.5 and the smallest for SSP2-4.5 for both the mean and extreme scenario.
iii. A higher magnitude of change was observed for flood depths compared to the spatial extent of the flood. The area inundated with water depths above 0.3 m increased with a higher magnitude for the mean events, and the area inundated with water depths above 0.5 m increased with a higher magnitude for the extreme events.
iv. Extreme SSP scenarios resulted in greater magnitude of change in flood extent and depth than the mean scenarios for both precipitation-induced flood and coastal flooding.

Despite current uncertainties about SLR projections, the area currently submerged at high tide is very likely to increase by 2080. This implies that new areas will become exposed to land loss, saline intrusion, and coastal flooding from compound effects. The study also showed that areas inundated with water depths above 0.5 m will become more frequent with future extreme rainfalls, and that water depths could increase to values that are not observed today. These findings suggest an increased exposure to flood related hazards and damage to housing, health,

and economy for the coastal population, along with increased socioeconomic and economic consequences on a country level.

More research that incorporates the effects of coastal erosion is needed to estimate the inundated areas more accurately at high tide. Further studies could additionally assess flooding in central coastal Bangladesh while including additional hydrological components such as river dynamics, storm surge, and wave interaction. A sensitivity analysis, which was restricted due to time constraints, could additionally be performed on this rural landscape using the TFM-DYN input variables. One of the major issues with accurate flood modelling is the availability of high-resolution elevation data, which was one of the greatest limitations in this study. The demand for a freely available DEM with high vertical and horizontal resolution remains and is crucial for mapping overland flow and accumulation and coastal flooding in flat landscapes such as coastal Bangladesh.

References

Anderson, T., Fletcher, C., Barbee, M., Romine, B., Lemmo, S., & Delevaux, J. (2018). Modeling multiple sea level rise stresses reveals up to twice the land at risk compared to strictly passive flooding methods. *Scientific Reports, 8*. https://doi.org/10.1038/s41598-018-32658-x Bangladesh Meteorological Department. (2016). *Daily Total Rainfall Till Jun 2014* [Data set]. http://data.gov.bd/dataset/daily-total-rainfall-till-jun-2014

Asian Development Bank. (2021, December 21). *Bangladesh Climate and Disaster Risk Atlas: Hazards* (Volume 1). Planning Commission, Ministry of Planning and Asian Development Bank. DOI: http://dx.doi.org/10.22617/TCS210518

Bangladesh Bureau of Statistics. (2021, May 14). *Statistical Year Book Bangladesh 2020* (40th Edition). Statistics & Information Division (SID), Ministry of Planning. Government of the People's Republic of Bangladesh. ISBN-978-984-475-047-0. http://www.bbs.gov.bd/site/page/29855dc1-f2b4-4dc0-9073-f692361112da/Statistical-Yearbook

Becker, M., Papa, F., Karpytchev, M., Delebecque, C., Krien, Y., Khan, J. U., Ballu, V., Durand, F., Cozannet, G. L., Islam, A. K. M. S., Calmant, S., & Shum, C. K. (2020). Water level changes, subsidence, and sea level rise in the Ganges-Brahmaputra-Meghna delta. *Proceedings of the National Academy of Sciences of the United States of America, 117*(4), 1867-1876. https://doi.org/10.1073/pnas.1912921117

Bricheno, L. M., & Wolf, J. (2018). Modelling tidal river salinity in coastal Bangladesh. In: Nicholls, R., Hutton, C., Adger, W., Hanson, S., Rahman, M., Salehin, M. (eds) Ecoysytem Services for Well-being Deltas. Palgrave Macmillan, Cham. 10.1007/978-3-319-71093-8_17

Bricheno, L. M., Wolf, J., & Sun, Y. (2021). Saline intrusion in the Ganges-Brahmaputra-Meghna megadelta. *Estuarine, Coastal and Shelf Science, 252*. https://doi.org/10.1016/j.ecss.2021.107246

Brouwer, C., Prins, K., Kay, M., & Heibloem, M. (1990). *Irrigation Water Management: Irrigation Methods* (No. 5). Food and Agriculture Organization of the United Nations Land and Water Development Division. https://www.fao.org/publications/card/en/c/b05e7149-50e2-51b0-b02a-d53eed1eb4cd

Brown, S., Nicholls, R. J., Lázár, A. N., Hornby, D. D., Hill, C., Hazra, S., Addo, K. A., Haque, A., Caesar, J., & Tompkins, E. L. (2018). What are the implications of sea-level rise for a 1.5, 2 and 3 °C rise in global mean temperatures in the Ganges-Brahmaputra-Meghna and other vulnerable deltas? *Regional Environmental Change, 18,* 1829–1842. https://doi.org/10.1007/s10113-018-1311-0

Caldwell, P. C., Merrifield, M. A., & Thompson, P. R. (2015). *Sea level measured by tide gauges from global oceans — the Joint Archive for Sea Level holdings* (Version 5.5) [Data set]. NOAA National Centers for Environmental Information. doi:10.7289/V5V40S7W.http://uhslc.soest.hawaii.edu/data/?rq#uh139a

Center for International Earth Science Information Network. (2018). *Gridded Population of the World: Population Density* (Version 4, Revision 11) [Data set]. NASA Socioeconomic Data and Applications Center. https://doi.org/10.7927/H49C6VHW

Climate Change Knowledge Portal. (2021). *Climate Data: Bangladesh*. World Bank. Retrieved on March 28, 2022, from https://climateknowledgeportal.worldbank.org/

Dasgupta, S., Hossain, M. M., Huq, M., & Wheeler, D. (2018). Climate Change, Salinization and High-Yield Rice Production in Coastal Bangladesh. *Agricultural and Resource Economics Review, 47*(1), 66-89. https://doi.org/10.1017/age.2017.14

Dasgupta, S., Huq, M., Khan, Z., Masud, M., Murshed, A., Mukherjee, N., & Pandey, K. (2010). *Climate Proofing Infrastructure in Bangladesh: The Incremental Cost of Limiting Future Inland Monsoon Flood Damage.* World Bank. https://openknowledge.worldbank.org/handle/10986/3950

Dasgupta, S., Zaman, A., Roy, S., Huq, M., Jahan, S., & Nishat, A. (2015). *Urban Flooding of Greater Dhaka in a Changing Climate: Building Local Resilience to Disaster Risk.* Directions in Development--Environment and Sustainable Development. World Bank. https://openknowledge.worldbank.org/handle/10986/22768

Dastagir, M. R. (2015). Modeling recent climate change induced extreme events in Bangladesh: A review. *Weather and Climate Extremes, 7*, 49-60. https://doi.org/10.1016/j.wace.2014.10.003

Earth Resources Observation and Science Center. (2018). *Shuttle Radar Topography Mission (SRTM) - Mission Summary*. Retrieved March 16, 2022, from https://www.usgs.gov/centers/eros/science/usgs-eros-archive-digital-elevation-srtm-mission-summary?qt-science_center_objects=0#overview

Elkhrachy, I. (2018). Vertical accuracy assessment for SRTM and ASTER Digital Elevation Models: A case study of Najran city, Saudi Arabia. *Ain Shams Engineering Journal, 9*(4), 1807-1817. https://doi.org/10.1016/j.asej.2017.01.007

Environmental Systems Research Institute. (2020). *ArcGIS Pro* (Version 2.7.0) [Computer software]. Esri Inc. https://www.esri.com/en-us/arcgis/products/arcgis-pro/overview.

Environmental Systems Research Institute. (n.d.). *Resample (Data Management)*. Retrieved March 25, 2022, from https://pro.arcgis.com/en/pro-app/2.8/tool-reference/data-management/resample.htm

European Space Agency. (2020). *Sentinel-2A* [Data set]. European Commission's Earth Observation Programme. /10.5066/F76W992G. Retrieved April 4, 2022, from https://earthexplorer.usgs.gov/

Food and Agriculture Organization of the United Nations. (2003). *The Digital Soil Map of The World* (Version 3.6) [Data set]. Land and Water Development Division, Rome. https://data.review.fao.org/map/catalog/srv/api/records/446ed430-8383-11db-b9b2-000d939bc5d8

Food and Agriculture Organization of the United Nations. (n.d.). *FAO Regional Office for Asia and the Pacific: Bangladesh.* Retrieved April 19, 2022, from https://www.fao.org/asiapacific/perspectives/agricultural-statistics/global-strategy/results-in-the-region/bangladesh/en/

Gesch, D. B. (2018). Best Practices for Elevation-Based Assessments of Sea-Level Rise and Coastal Flooding Exposure. *Frontiers in Earth Science, 6*. https://doi.org/10.3389/feart.2018.00230

Google. (n.d.). *Google Earth Pro (Version 7.3)* [Computer software]. https://www.google.com/earth/versions/

Gutiérrez, J. M., Jones, R.G., Narisma, G.T., Alves, L.M., Amjad, M., Gorodetskaya, I.V., Grose, M., Klutse, N.A.B., Krakovska, S., Li, J., Martínez-Castro, D., Mearns, L.O., Mernild, S.H., Ngo-Duc, T., van den Hurk, B., & Yoon, J.-H. (2021). *Atlas. In Climate Change 2021: The Physical Science Basis. Contribution of Working Group I to the Sixth Assessment Report of the Intergovernmental Panel on Climate Change* [Masson-Delmotte, V., P. Zhai, A. Pirani, S.L. Connors, C. Péan, S. Berger, N. Caud, Y. Chen, L. Goldfarb, M.I. Gomis, M. Huang, K. Leitzell, E. Lonnoy, J.B.R. Matthews, T. K., Maycock, T. Waterfield, O. Yelekçi, R. Yu, and B. Zhou (eds.)]. Cambridge University Press. In Press. Interactive Atlas available from Available from http://interactive-atlas.ipcc.ch/

Hasan, M. K., Kumar, L., & Gopalakrishnan, T. (2020). Inundation modelling for Bangladeshi coasts using downscaled and bias-corrected temperature. *Climate Risk Management, 27*. https://doi.org/10.1016/j.crm.2019.100207

Huq, S. M. I., & Shoaib, J. U. M. (2013). *The Soils of Bangladesh* (1st ed.). Springer Dordrecht. https://doi.org/10.1007/978-94-007-1128-0

IPCC. (2021). *Climate Change 2021: The Physical Science Basis. Contribution of Working Group I to the Sixth Assessment Report of the Intergovernmental Panel on Climate Change* [Masson-Delmotte, V., P. Zhai, A. Pirani, S.L. Connors, C. Péan, S. Berger, N. Caud, Y. Chen, L. Goldfarb, M.I. Gomis, M. Huang, K. Leitzell, E. Lonnoy, J.B.R. Matthews, T.K. Maycock, T. Waterfield, O. Yelekçi, R. Yu, & B. Zhou (eds.)]. Cambridge University Press. In Press. https://www.ipcc.ch/report/ar6/wg1/

Iturbide, M., Fernández, J., Gutiérrez, J.M., Bedia, J., Cimadevilla, E., Díez-Sierra, J., Manzanas, R., Casanueva, A., Baño-Medina, J., Milovac, J., Herrera, S., Cofiño, A.S., San Martín, D., García-Díez, M., Hauser, M., Huard, D., & Yelekci, Ö. (2021). *Repository supporting the implementation of FAIR principles in the IPCC-WG1 Atlas.* Zenodo, DOI: 10.5281/zenodo.3691645. Available from: https://github.com/IPCC-WG1/Atlas

Mattocks, C., & Forbes, C. (2008). A real-time, event-triggered storm surge forecasting system for the state of North Carolina. *Ocean Modelling, 25*(3), 95-119. https://doi.org/10.1016/j.ocemod.2008.06.008

Ministry of Foreign Affairs of the Netherlands. (2018, April). *Climate Change Profile: Bangladesh* (Report 17BUZ108158). Government of the Netherlands. https://www.government.nl/documents/publications/2019/02/05/climate-change-profiles

Murshed, S. B., Islam, A. K. M., & Khan, M. S. A. (2011). Impact of Climate Change on Rainfall Intensity in Bangladesh. *3rd International Conference on Water & Flood Management, Dhaka.* https://citeseerx.ist.psu.edu/viewdoc/download?doi=10.1.1.716.8645&rep=rep1&type=pdf

Na, W., & Yoo, C. (2018). Evaluation of rainfall temporal distribution models with annual maximum rainfall events in Seoul, Korea. *Water, 10*(10), 1468. https://doi.org/10.3390/w10101468

Nandargi, S., & Mulye, S. S. (2012). Relationships between Rainy Days, Mean Daily Intensity, and Seasonal Rainfall over the Koyna Catchment during 1961–2005. *The Scientific World Journal, 2012*. https://doi.org/10.1100/2012/894313

NASA JPL. (2013). *NASA Shuttle Radar Topography Mission Global 1 arc second* (Version 3) [Data set]. NASA EOSDIS Land Processes DAAC. https://doi.org/10.5067/MEaSUREs/SRTM/SRTMGL1.003

Nicholls, R. J., Hutton, C. W., Adger, W. N., Hanson, S. E., Rahman, M. M., & Salehin, M. (2018). *Ecosystem Services for Well-Being in Deltas. Integrated Assessment for Policy Analysis*. Springer International Publishing. https://doi.org/https://doi-org.ludwig.lub.lu.se/10.1007/978-3-319-71093-8

Nilsson, H., Pilesjo, P., Hasan, A., & Persson, A. (2021). Dynamic spatio-temporal flow modeling with raster DEMs. *Transactions in GIS, 00*, 1– 17. https://doi.org/10.1111/tgis.12870

Papaioannou, G., Vasiliades, L., Loukas, A., Efstratiadis, A., Koukouvinos, A., Tsoukalas, I., Kossieris, P., & Papalexiou, S. M. (2018). An operational method for Flood Directive implementation in ungauged urban areas. *Hydrology, 5*(2). https://doi.org/10.3390/hydrology5020024

Pekel, J.-F., Cottam, A., Gorelick, N., & Belward, A. S. (2016). High-resolution mapping of global surface water and its long-term changes. *Nature, 540*(7633), 418-422. https://doi.org/10.1038/nature20584

Pilesjö, P., & Hasan, A. (2014). A triangular form-based multiple flow algorithm to estimate overland flow distribution and accumulation on a digital elevation model. *Transactions in GIS MECW: The Middle East in the Contemporary World eSSENCE: The e-Science Collaboration, 18*(1), 108-124. https://doi.org/10.1111/tgis.12015

Pingping, H., Xue, S., Li, P., & Zhanbin, L. (2013). Effect of vegetation cover types on soil infiltration under simulating rainfall. *Nature Environment and Pollution Technology, 12*, 193-198. https://neptjournal.com/upload-images/NL-42-2-2.pdf

Rabby, Y. W., Ishtiaque, A., & Rahman, M. S. (2020). Evaluating the Effects of Digital Elevation Models in Landslide Susceptibility Mapping in Rangamati District, Bangladesh. *Remote Sensing, 12*(2718), 2718-2718. https://doi.org/10.3390/rs12172718

Rasel, M. M., & Chowdhury, M. T. U. (2015). Modeling Rainfall Intensity Duration Frequency (R-IDF) Relationship for Seven Divisions of Bangladesh. *European Academic Reseearch, 3*(5), 5784–5801. https://www.euacademic.org/UploadArticle/1900.pdf

Riahi, K., van Vuuren, D. P., Kriegler, E., Edmonds, J., O'Neill, B. C., Fujimori, S., Bauer, N., Calvin, K., Dellink, R., Fricko, O., Lutz, W., Popp, A., Cuaresma, J. C., Kc, S., Leimbach, M., Jiang, L., Kram, T., Rao, S., Emmerling, J., … Tavoni, M. (2017). The Shared Socioeconomic Pathways and their energy, land use, and greenhouse gas emissions implications: An overview. *Global Environmental Change, 42*, 153-168. https://doi.org/https://doi.org/10.1016/j.gloenvcha.2016.05.009

Roy, B., Khan, M. S. M., Saiful Islam, A. K. M., Mohammed, K., & Khan, M. J. U. (2021). Climate-induced flood inundation for the Arial Khan River of Bangladesh using open-source SWAT and HEC-RAS model for RCP8.5-SSP5 scenario. *SN Applied Sciences, 3*(6), 1-13. https://doi.org/10.1007/s42452-021-04460-4

Sentinel Hub. (n.d.). *Airbus Pleiades and Airbus SPOT.* Sentinel Hub by Sinergise. Retrieved April 14, 2022, from https://docs.sentinel-hub.com/api/latest/data/

Shamsudduha, M., Marzen, L., Uddin, A., Lee, M.-K., & Saunders, J. (2008). Spatial relationship of groundwater arsenic distribution with regional topography and water-table fluctuations in the shallow aquifers in Bangladesh. *Environmental Geology, 57*, 1521-1535. https://doi.org/10.1007/s00254-008-1429-3

Shelley, I. J., Takahashi-Nosaka, M., Kano-Nakata, M., S. Haque, M., & Inukai, Y. (2016). Rice Cultivation in Bangladesh: Present Scenario, Problems, and Prospects. *Journal of International Cooperation for Agricultural Development, 14*, 20-29. https://doi.org/10.50907/jicad.14.0_20

Smith-Konter, B., & Sandwell, D. (2003). Accuracy and Resolution of Shuttle Radar Topography Mission Data. *Geophysical Research Letters, 30*. https://doi.org/10.1029/2002GL016643

Uddin Komol, M. K. (2011). *Numerical Simulation of Tidal Level At Selected Coastal Area of Bangladesh* [M.S. thesis, Bangladesh University of Engineering and Technology (BUET)]. BUET Central Library. http://lib.buet.ac.bd:8080/xmlui/handle/123456789/150

Wang, Y., Zhang, B., & Banwart, S. A. (2017). Chapter Three - Reduced Subsurface Lateral Flow in Agroforestry System Is Balanced by Increased Water Retention Capacity: Rainfall Simulation and Model Validation. *Advances in Agronomy, 142*, 73-97. https://doi.org/10.1016/bs.agron.2016.10.005

World Resources Institute. (2020). *Aqueduct Floods Hazard Maps* (Version 2) [Data set]. https://www.wri.org/data/aqueduct-floods-hazard-maps

Yang, B., Heo, H. K., Lee, D. K., & Biging, G. (2019). The effects of tree characteristics on rainfall interception in urban areas. *Landscape and Ecological Engineering, 15*(3), 289-296. https://doi.org/10.1007/s11355-019-00383-w

Yao, J., Chao-lu, Y., & Ping, F. (2020). Evaluation of the Accuracy of SRTM3 and ASTER GDEM in the Tibetan Plateau Mountain Ranges. *E3S Web of Conferences, 206*, https://doi.org/10.1051/e3sconf/202020601027

Appendix A

Estimation of high tide

The maximum difference in sea level between high tide and mean sea level in July 1980 – 2000. The years 1986 and 1993 are excluded due to missing data in July (9 and 11 days respectively), and the remaining years are combined into a mean that is used in the analysis.

Year	Contribution of high tide (m)
1980	1.797
1981	1.599
1982	1.686
1983	1.703
1984	2.026
1985	1.768
1986	-
1987	2.041
1988	1.875
1989	1.686
1990	1.577
1991	1.706
1992	2.051
1993	-
1994	1.984
1995	2.100
1996	1.979
1997	1.674
1998	1.979
1999	1.776
2000	1.694
Mean (1980-2000)	1.826

Appendix B

Simulation setup

Values for precipitation and coastline change used in each simulation. Change in coastline incorporates the influence of high tide and relative sea level rise.

Scenario	Total precipitation (mm)	Change in coastline (m)
Baseline Mean	19	1.8
SSP2-4.5 Mean	20	2.7
SSP3-7.0 Mean	21	2.8
SSP5-8.5 Mean	23	2.9
Baseline Extreme	90	1.8
SSP2-4.5 Extreme	108	3.1
SSP3-7.0 Extreme	124	3.2
SSP5-8.5 Extreme	170	3.3

Appendix C

Flood maps

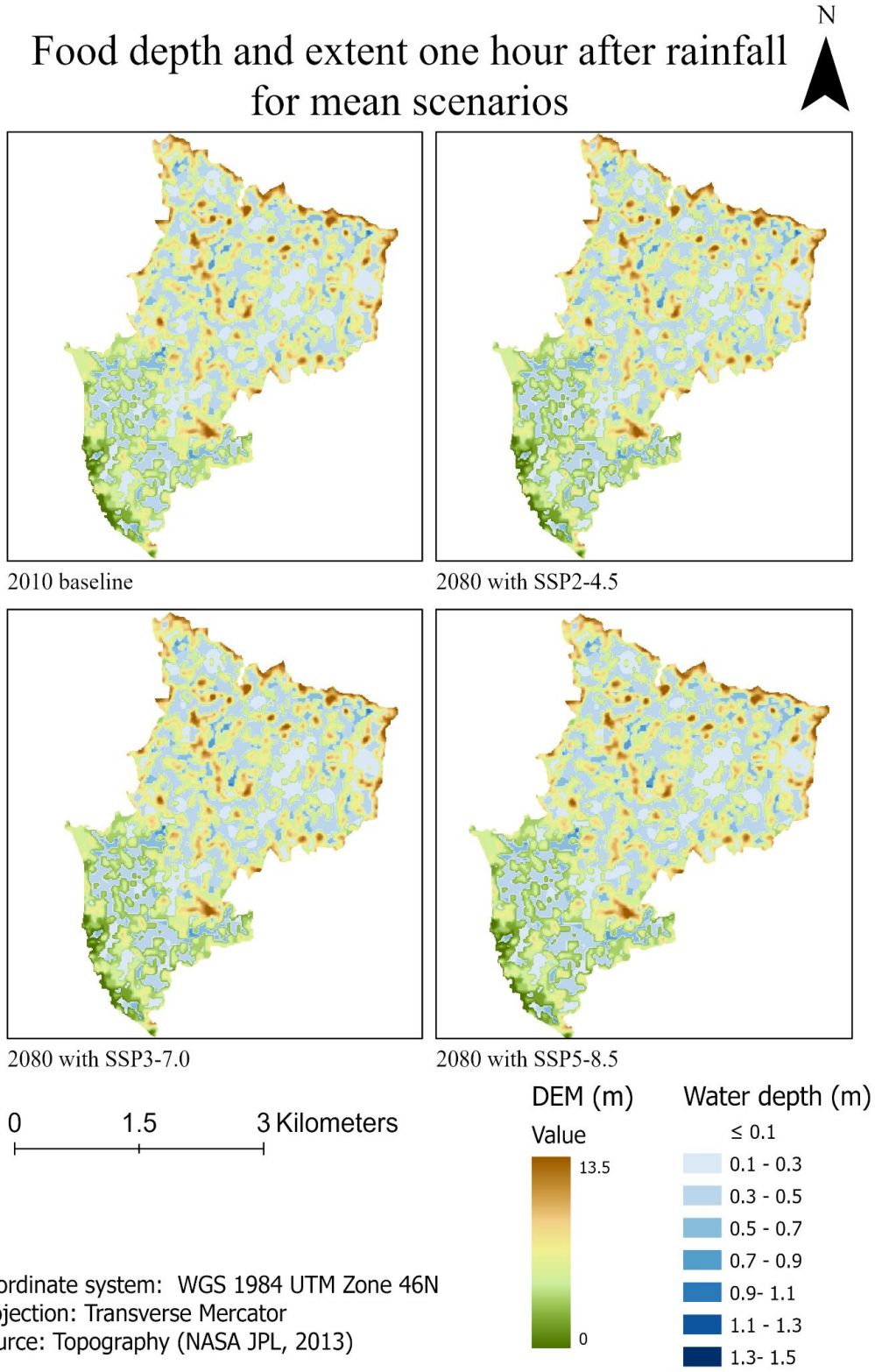

Figure C1. Flood depth and extent one hour after rainfall (13 hours) for all mean scenarios. Water depths are visualized ranging from low (light blue) to high (dark blue) on top of elevation data from low elevations (green) to high elevation (red).

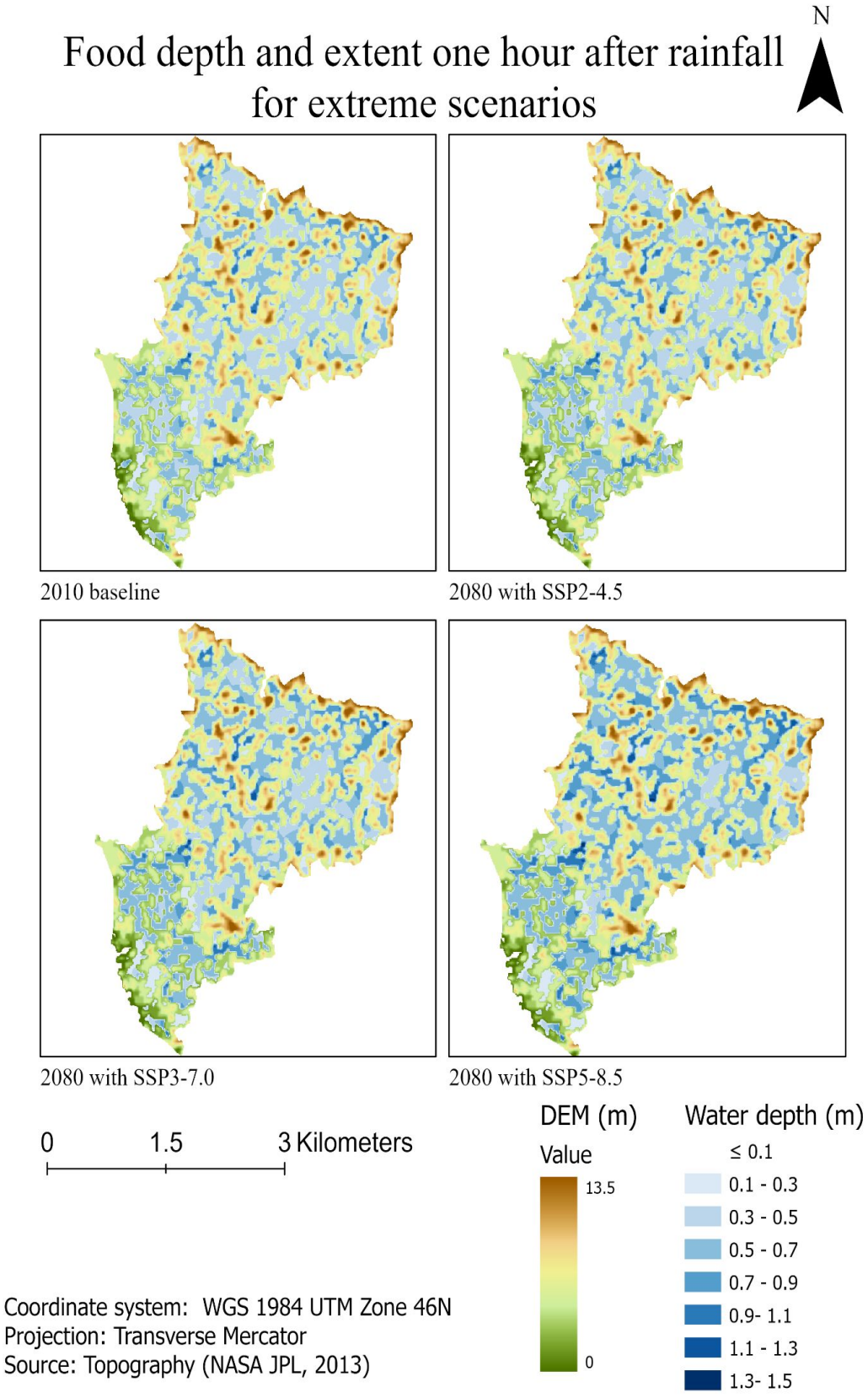

Figure C2. Flood depth and extent one hour after rainfall (13 hours) for all extreme scenarios. Water depths are visualized ranging from low (light blue) to high (dark blue) on top of elevation data from low elevations (green) to high elevation (red).

Appendix D

Precipitation-induced flood depth and extent

Table D1. Area inundated per flood depth at mid rainfall (6 hours) for mean events.

Inundation depth (m)	Baseline scenario (ha)	SSP2-4.5 (ha)	SSP3-7.0 (ha)	SSP5-8.5 (ha)
0.1 - 0.3	264.6	265.2	265.6	267.0
0.3 - 0.5	20.5	21.2	21.6	22.7
0.5 - 0.7	1.3	1.3	1.4	1.5
0.7 - 0.9	0.1	0.1	0.1	0.1

Table D2. Area inundated per flood depth at mid rainfall (6 hours) for extreme events.

Inundation depth (m)	Baseline scenario (ha)	SSP2-4.5 (ha)	SSP3-7.0 (ha)	SSP5-8.5 (ha)
0.1 - 0.3	251.1	236.6	220.3	172.0
0.3 - 0.5	77.1	97.2	117.5	167.5
0.5 - 0.7	8.6	11.6	15.0	30.7
0.7 - 0.9	0.8	1.0	1.7	3.9
0.9 - 1.1	0.0	0.0	0.1	0.5

Table D3. Area inundated per flood depth at end of rainfall (12 hours) for mean events.

Inundation depth (m)	Baseline scenario (ha)	SSP2-4.5 (ha)	SSP3-7.0 (ha)	SSP5-8.5 (ha)
0.1 - 0.3	167.1	164.7	163.4	158.6
0.3 - 0.5	157.5	159.8	160.9	165.0
0.5 - 0.7	21.6	22.3	23.1	24.9
0.7 - 0.9	2.6	2.6	2.8	3.0
0.9 - 1.1	0.1	0.1	0.1	0.2

Table D4. Area inundated per flood depth at end of rainfall (12 hours) for extreme events.

Inundation depth (m)	Baseline scenario (ha)	SSP2-4.5 (ha)	SSP3-7.0 (ha)	SSP5-8.5 (ha)
0.1 - 0.3	85.1	81.5	79.9	75.9
0.3 - 0.5	187.1	163.4	141.9	92.9
0.5 - 0.7	99.4	122.9	141.2	173.9
0.7 - 0.9	18.3	28.9	40.4	72.7
0.9 - 1.1	2.9	4.1	5.6	15.9
1.1 - 1.3	0.1	0.4	0.8	2.2
1.3 - 1.5	0.0	0.0	0.0	0.1

Table D5. *Area inundated per flood depth one hour after rainfall (13 hours) for mean events.*

Inundation depth (m)	Baseline scenario (ha)	SSP2-4.5 (ha)	SSP3-7.0 (ha)	SSP5-8.5 (ha)
0.1 - 0.3	143.9	141.9	139.0	135.6
0.3 - 0.5	176.5	178.0	179.4	182.7
0.5 - 0.7	30.7	31.7	32.8	34.7
0.7 - 0.9	3.4	3.5	3.6	3.7
0.9 - 1.1	0.3	0.3	0.3	0.4

*Table D*6. *Area inundated per flood depth one hour after rainfall (13 hours) for extreme events.*

Inundation depth (m)	Baseline scenario (ha)	SSP2-4.5 (ha)	SSP3-7.0 (ha)	SSP5-8.5 (ha)
0.1 - 0.3	82.7	79.9	78.4	74.3
0.3 - 0.5	171.2	146.1	122.7	86.7
0.5 - 0.7	115.4	135.9	154.0	170.3
0.7 - 0.9	23.2	36.8	48.8	81.7
0.9 - 1.1	3.5	5.0	7.3	19.0
1.1 - 1.3	0.3	0.6	1.1	2.7
1.3 - 1.5	0.0	0.0	0.0	0.2

*Table D*7. *Flood extent (depths > 0.1) throughout and after mean rainfall events. Mid rainfall occurs at 6 hours, end of rainfall at 12 hours, and one after rainfall at 13 hours.*

Time (hours)	Baseline scenario (ha)	SSP2-4.5 (ha)	SSP3-7.0 (ha)	SSP5-8.5 (ha)
6	286.4	0.5	0.8	1.7
12	348.8	0.2	0.4	0.8
13	354.7	0.2	0.4	0.7

*Table D*8. *Flood extent (depths > 0.1) throughout and after extreme rainfall events. Mid rainfall occurs at 6 hours, end of rainfall at 12 hours, and one after rainfall at 13 hours.*

Time (hours)	Baseline scenario (ha)	SSP2-4.5 (ha)	SSP3-7.0 (ha)	SSP5-8.5 (ha)
6	337.6	2.6	5.0	11.0
12	392.9	2.1	4.3	10.4
13	396.2	2.0	4.1	9.8